eman ta zabal zazu
Universidad del País Vasco
Euskal Herriko Unibertsitatea
ZIENTZIA ETA TEKNOLOGIA FAKULTATEA
FACULTAD DE CIENCIA Y TECNOLOGÍA

Gradu Amaierako Lana / Trabajo Fin de Grado
Gradu bikoitza Fisikan eta Ingeniaritza Elektronikoan
/ Doble Grado en Física y en Ingeniería Electrónica

Seeking topological phase transition applying pressure to Ag_3AuSe_2 and Ag_3Te_2Au

Egilea/Autor/a:
Arkaitz Bidaurrazaga Barrueta
Zuzendaria/Director/a:
Aitor Bergara Jauregi
Zuzendarikideaa/Codiirector/a:
Maia Garcia Vergniory

Leioa, 2019ko ekainaren 20a /Leioa, 20 de junio de 2019

Contents

Chapter 1

Introduction

For many years the Solid State Physics has contributed significantly to the modern society, giving a profound understanding of how semiconductors behave, which led to a revolution with the improvement of transistors. Furthermore, the striking advances in computation have assisted to solve numerically heavy calculus, such as the ones arisen from Quantum Theory, which includes calculations regarding crystals.

Recently, a whole new field of Solid State Physics has arisen, the Topological Materials, but we will focus on the Topological Insulators (TI). A topological insulator is a material with non-trivial symmetry-protected topological order that behaves as an insulator in its interior but whose surface contains conducting states, meaning that electrons can only move along the surface of the material. However, having a conducting surface is not unique to topological insulators, since ordinary band insulators can also support conductive surface states. What makes TI special is that their surface states are symmetry-protected by particle number conservation and time-reversal symmetry. Topological insulators are characterized by an index (known as $\mathbb{Z}_2$ topological invariants) similar to the genus[1] in topology. As long as time-reversal symmetry is preserved, in other words, as long as there is no magnetism, the $\mathbb{Z}_2$ index cannot change by small perturbations and the conducting states at the surface are symmetry-protected. A brand new way to study TI is presented in the literature [1], where they use Group Theory in order to determine the topology of crystals.

One important property of these topological invariants is that they are robust against perturbations. In a few years, different phases displaying topological properties have been found: topological insulators, Weyl semimetals and non symmorphic materials whose electric properties are protected by time reversal symmetry or some crystalline symmetry. A Weyl node is basically a band crossing close to the Fermi level, where the dispersion is linear and is protected by time reversal or inversion symmetry. Consequently, the charge carriers, responsible for electrical conduction, can be considered as massless fermions, supported theoretically by the Dirac equation.

The main objective of this project is to seek topological materials, for this purpose we will study two crystals, Ag_3AuSe_2 and Ag_3Te_2Au. These materials are trivial insulators under zero pressure, therefore, we will apply pressure to each material and calculate their band structure, with the information obtained from those calculations we will be able to determine if the material is topological or not, as we will explain in section B.

In this dossier we will start introducing topological matter, then we will explain some basics about the Density Functional Theory (DFT), and we will define some important concepts about topology, which are related with the topic of this project, such as representations and irreducible representations. Next we will expose some general properties of the materials we are studying (symmetry group, lattice parameters, band structure...). After that we will apply pressure to the materials and observe how the band structure changes, yielding to new topological properties. Finally, we will present some conclusions about the results we obtain.

[1] The genus of an orientable surface is the number of holes it has, so that a sphere has genus 0 and a torus has genus 1.

Chapter 2

Brief introduction of TI

The study of Topological Insulators began with a deeper understanding of the polarization and magnetization of crystalline materials. In this theoretical framework of solid state physics electromagnetism and quantum mechanics are two paramount pillars. When solving Schrödinger's equation for the electron distribution throughout a crystal, the resulting charge density peaks around the atomic positions, but it does not vanish between atoms. As a result, there is no natural way to decompose the electron charge into polarized units, equally, the same problem arises for magnetization.

With the discovery of quantum Hall effect (QHE) in 1980, which consists in applying a magnetic field at low temperature to a 2-dimensional electron gas, a transverse conductivity was measured in terms of quantized integers of e^2/h. This provided one of the first hints that concepts of quantization, invariance and topology may play an important role in condensed matter theory.

2.1 Polarization and surface charge density

The main problem with the old definition of polarization is that it is heavily dependent on which unit cell is chosen to calculate it,

$$\mathbf{P} = \frac{1}{V_{cell}} \int_{cell} \mathbf{r}\rho(\mathbf{r}) d\mathbf{r} \tag{2.1}$$

where $\rho(\mathbf{r})$ is the charge density, which due to translational symmetry is periodic in the crystal, thus the main issue comes from the ill defined $\mathbf{r}$ operator, because it is not periodic at all. One suggestion could be to average over all possible unit cell locations, but unfortunately the result of this procedure is always exactly zero, which is useless.

Now we consider a static situation in which a crystalline insulator with polarization $\mathbf{P}$ has a surface normal to $\hat{\mathbf{n}}$. We expect a bound charge on the surface, related to $\mathbf{P}$ by,

$$\sigma_{surf} = \mathbf{P} \cdot \hat{\mathbf{n}} \tag{2.2}$$

where σ_{surf} is the macroscopic surface charge density. However, this relation is not accurate enough, the real form is demonstrated in chapter 1 of [2] to be the following one:

$$\sigma_{surf} := \mathbf{P} \cdot \hat{\mathbf{n}} \tag{2.3}$$

The special notation ":=" (introduced by Vandelbrit and Resta in 2006) means that the object on the left-hand side is equal to one of the values on the right hand side, where $\mathbf{P} \cdot \hat{\mathbf{n}}$ is interpreted as a multivalued object whose values are separated by the lattice values of e/A_{surf}, being A_{surf} the area of the surface where the charge resides. Evidently, $\hat{\mathbf{n}}$ is uniquely defined, therefore $\mathbf{P}$ carries the branch-choice uncertainty. For this argument to work, $\mathbf{P}$ must be defined modulo a 3D lattice value:

$$\Delta\mathbf{P} = \frac{e\mathbf{R}}{V_{cell}} \tag{2.4}$$

Where $\mathbf{R}$ is a lattice vector, since $\Delta\mathbf{P} \cdot \hat{\mathbf{n}} = \frac{e(\hat{\mathbf{n}}\cdot\mathbf{R})}{V_{cell}} = \frac{me}{A_{cell}}$ (m an integer) is satisfied.

2.2 Polarization and Berry phase

In 1990 the electromagnetic structure community was able to calculate derivatives of $\mathbf{P}$, but not $\mathbf{P}$ itself. This paradox was resolved with the arrival of a new theory of polarization based on Berry phases. The Berry phase is the dynamical phase an electron acquires after a closed loop, where the path lies within the wavector space $\mathbf{k}$ and the phase is related to the electron quantum state in the crystal.

Without going into further detail, it was proven that the polarization is related to the Berry phase (see a further explanation in 3). This relation is demonstrated in depth in the literature [2, 3]. For example, with a cubic cell the polarization has the form,

$$\mathbf{P} = -\frac{e}{V_{cell}} \sum_j \frac{\overline{\phi}_j}{2\pi} \mathbf{a}_j \tag{2.5}$$

where $j = 1, 2, 3$ indicates the direction x, y, z in which the Berry phase was calculated respectively, and $\mathbf{a}_j$ are the real space lattice vectors. Each berry phase is not gauge invariant, therefore they are undetermined by modulo 2π: $\overline{\phi}_j \to \overline{\phi}_j + 2\pi m_j$. As a consequence, we obtain the uncertainty of $\mathbf{P}$ introduced in 2.4, $\Delta\mathbf{P} = \frac{e\mathbf{R}}{V_{cell}}$, being $\mathbf{R} = -\sum_j m_j \mathbf{a}_j$.

2.3 Group theory, a new framework

Crystalline materials consist of ordered arrays of atoms at lattice sites, with electrons in local orbitals that hybridize and determine many physical properties of the material. Due to the non-vanishing overlap of orbitals, the Hamiltonian contains terms coupling different lattice sites. Therefore, the real-space Hamiltonian is not diagonal in real space. Although the chemical description and many physical properties are local, physicists have chosen to understand crystals using band theory, because the Hamiltonian is diagonal in momentum space. The momentum space picture, while extremely useful, also obfuscates the local physics present in crystals.

To remedy this disconnect, Zak introduced the concept of a band representation (BR) for spinless systems, with and without time-reversal symmetry [4]. These band representations are, speaking generally, mathematical vehicles that relate the orbital representation of electrons on sites in real space to the momentum space description of the electron bands in the Brillouin zone. Zak realized that band representations can be decomposed into 'elementary building bricks', which are themselves band representations, but which cannot be further subdivided while preserving the symmetry operations of the system. Physically, the Elementary Band Representation (EBR) connectivity represents the number of energy bands that are connected together in the Brillouin zone, and which cannot be disconnected without breaking the space-group symmetry of the crystal.

In order to determine the properties of the BR Group theory is needed, with Group theory we are able to compute how each BR decomposes in different EBR on each point within the Brillouin zone. Among this, a local description[1] of atomic orbitals induces a global description of the band structure that determines a local $\mathbf{k} \cdot \mathbf{p}$ description at every point in momentum space.

In this work we have chosen to study the materials Ag_3AuSe_2 and Ag_3Te_2Au for many reasons. First of all, they have a clean band structure under zero pressure, and they are trivial insulators. On the other hand, their space group is a chiral group[2] which could lead to the quantized Circular Photo-galvanic Effect (CPGE) presented in [6]. The CPGE is the contribution to the optical response that switches sign when reversing the sense of the polarization of light. Second order nonlinear effects require the breaking of inversion symmetry, a condition that permits the existence of topologically charged Weyl points, and both materials have no inversion symmetry. Furthermore, they have a small gap which is manageable with the pressure, this way we pretend to close the gap around the Fermi level in order to get Weyl nodes and obtain topological bands.

[1] Mathematically, a site-symmetry group representation.

[2] Chiral groups are space groups that only contain pure rotations, they do not contain any mirror or inversion.

Chapter 3

Berry phase and Chern theorem

Our goal here is to introduce the concept of the Berry phase and explain how it enters into the quantum-mechanical band theory of electrons in crystals. We will begin by introducing the Berry phase in its abstract mathematical form, and then discuss its application to the adiabatic dynamics of finite quantum systems.

Definition: A Berry phase is a phase[1] that describes a global phase evolution of a complex vector[2] while is carried around a path in its vector space.

As we are interested only in the phase, we will suppose our complex vectors are unitary, and we will identify them with a ground-state wavefuntion of some Hamiltonian. First of all, we will give the formulation for the discrete case, ergo there will be N finite vectors, labelled as $|u_i\rangle$ and being $|u_0\rangle \equiv |u_N\rangle$. Then the Berry phase is defined to be,

$$\phi = -Im \ln[\prod_{i=0}^{N-1} \langle u_i | u_{i+1} \rangle] \ (mod\ 2\pi) \tag{3.1}$$

with this definition all the phase differences between the neighbours vectors are summed up, returning the global phase variation, with the branch choice of $Im \ln z \in [0, 2\pi)$. Recall that for a complex number $z = |z|e^{i\varphi}$ the expression $Im \ln z = \varphi$ gives the phase of said number, ignoring the magnitude.

It is easily demonstrated that the Berry phase is independent of the choices made for the phases of the individual $|u_i\rangle$. Suppose that we define a new vector set:

$$|\tilde{u}_i\rangle = e^{-i\beta_i} |u_i\rangle \ \ ; \ \beta_i \in \mathbb{R} \tag{3.2}$$

This transformation is called a Gauge transformation, and leaves ϕ invariant, because each vector $|\tilde{u}_i\rangle$ appears as bra and ket in the equation 3.1 therefore the added phase cancels with its conjugate. Thus the Berry phase is gauge invariant, which strongly hints that it may be related to some physically observable phenomena.

Another hint that the Berry phase formula above may be physically meaningful arises from the fact that it has a well-defined continuum limit. In the continuous formulation, we parametrize the vectors by a real variable $\lambda \to |u_\lambda\rangle$, where $|u_\lambda\rangle$ are assumed to be smooth and differentiable function of λ. Then the expression for the Berry phase is derived from 3.1:

$$\begin{aligned} \ln \langle u_\lambda | u_{\lambda + d\lambda} \rangle &= \ln \langle u_\lambda | \left(|u_\lambda\rangle + d\lambda \frac{d\,|u_\lambda\rangle}{d\lambda} + ... \right) \\ &= \ln(1 + d\lambda \langle u_\lambda | \partial_\lambda u_\lambda \rangle + ...) \\ &\simeq d\lambda \langle u_\lambda | \partial_\lambda u_\lambda \rangle \end{aligned} \tag{3.3}$$

[1] Berry phase is defined in the interval $\phi \in [0, 2\pi)$.

[2] Where the complex vector in question is a Bloch wavefunction (eigenstate of the Hamiltonian), and the path lies in the space of wavevectors $\mathbf{k}$ within the Brillouin zone.

In solid state physics the Berry phase is defined for each Bloch function, ergo each band has a Berry phase (with $|u_{n\mathbf{k}}(\mathbf{r})\rangle$, ϕ_n is the berry phase of the band n). Here λ can be any parameter, with any dimension. It can describe an adiabatic deformation, so the Berry phase will measure how the phase of the Bloch function is transformed throughout the adiabatic process, or it can also be the momentum $\mathbf{k}$ (3-dimensional) of the reciprocal space, then ϕ_n will describe how the phase of $|u_n(\mathbf{k})\rangle$ varies along a path ($\partial\Gamma$) in the reciprocal space. For simplicity, we will consider for now on that our parameter λ to be $\mathbf{k}$, and the vector set to be the Bloch states of a crystal $|u_{n\mathbf{k}}(\mathbf{r})\rangle$[3] presented in 5.26, where:

$$\begin{aligned} \hat{H}_{\mathbf{k}} &= e^{-i\mathbf{k}\cdot\mathbf{r}}\hat{H}e^{i\mathbf{k}\cdot\mathbf{r}} \\ \hat{H}_{\mathbf{k}}\,|u_{n\mathbf{k}}(\mathbf{r})\rangle &= E_{n\mathbf{k}}\,|u_{n\mathbf{k}}(\mathbf{r})\rangle \end{aligned} \tag{3.4}$$

Combining 3.1 and 3.3 we obtain the Berry phase in the continuous formulation:

$$\phi = -Im \oint_{\partial\Gamma} \langle u_\lambda|\partial_\lambda u_\lambda\rangle \, d\lambda \tag{3.5}$$

In fact it is easily proven that $\langle u_\lambda|\partial_\lambda u_\lambda\rangle$ is purely imaginary[4]. Hence:

$$\phi = i\oint_{\partial\Gamma} \langle u_\lambda|\partial_\lambda u_\lambda\rangle \, d\lambda = \oint_{\partial\Gamma} \langle u_{n\mathbf{k}}(\mathbf{r})|i\nabla_{\mathbf{k}}|u_{n\mathbf{k}}(\mathbf{r})\rangle \, d\mathbf{k} \equiv \phi_n \tag{3.6}$$

The integrand is known as the Berry connection or Berry potential:

$$A_n(\mathbf{k}) = \langle u_{n\mathbf{k}}(\mathbf{r})|i\nabla_{\mathbf{k}}|u_{n\mathbf{k}}(\mathbf{r})\rangle \tag{3.7}$$

When the path described in the integral is closed, then by Stocke's theorem, we can calculate the Berry phase with a surface integral:

$$\oint_{\partial\Gamma} A_n(\mathbf{k})d\mathbf{k} = \iint_{\Gamma} \nabla_{\mathbf{k}} \times A_n(\mathbf{k})d\mathbf{S} = \iint_{\Gamma} \Omega_n(\mathbf{k})d\mathbf{S} \tag{3.8}$$

Where $\partial\Gamma$ is the closed path, Γ is the surface described by C and $\Omega_n(\mathbf{k})$ is called the Berry curvature. But the Berry curvature is gauge-invariant[5], so it should be well defined without a modulo 2π the same as the Berry phase. Therefore the relation obtained above must be rewritten as[6]:

$$\iint_{\Gamma} \Omega_n(\mathbf{k})d\mathbf{S} := \oint_{\partial\Gamma} A_n(\mathbf{k})d\mathbf{k} \tag{3.9}$$

[3] In this section we use bracket notation. Notice that in this notation: $\langle u_{n'\mathbf{k}'}(\mathbf{r})|u_{n\mathbf{k}}(\mathbf{r})\rangle = \int \overline{u}_{n'\mathbf{k}'}(\mathbf{r})u_{n\mathbf{k}}(\mathbf{r})d\mathbf{r}$.

[4] $2Re\,\langle u_\lambda|\partial_\lambda u_\lambda\rangle = \langle u_\lambda|\partial_\lambda u_\lambda\rangle + \langle \partial_\lambda u_\lambda|u_\lambda\rangle = \partial_\lambda\,\langle u_\lambda|u_\lambda\rangle = 0$

[5] When we use a smooth gauge transformation, as can be seen in 3.1 the divergence of the curl of $\beta(\mathbf{k})$ will always be zero, making $\Omega_n(\mathbf{k})$ gauge-invariant.

[6] This formula resembles the equation 2.3, where the special character := is introduced.

In fact, as the curve $\partial\Gamma$ is in the surface of a 3D volume, two surfaces can be chosen (Γ_1 and Γ_2) and the Berry phases for each surface can be easily calculated, because they differ only by having reverse direction around $\partial\Gamma$. Consequently $\iint_{\Gamma_1} \Omega_n(\mathbf{k}) d\mathbf{S} = \phi_n$; $\iint_{\Gamma_2} \Omega_n(\mathbf{k}) d\mathbf{S} = -\phi_n$ and then the integral over the hole ($\Gamma = \Gamma_1 \cap \Gamma_2$) surface:

$$\oint_{\Gamma} \Omega_n(\mathbf{k}) d\mathbf{S} := 0 \tag{3.10}$$

Finally, we introduce the Chern Theorem, which states:

Chern Theorem: The integral of the Berry curvature over any closed 2D manifold is 2π times some integer:

$$\oint_{\Gamma} \Omega_n(\mathbf{k}) d\mathbf{S} = 2\pi C_n \ ; \ C_n \in \mathbb{Z} \tag{3.11}$$

This integer is known as the Chern number of the surface, and can be regarded as a topological index or topological invariant attached to the manifold of states $|u_n(\mathbf{k})\rangle$ defined over the closed surface Γ[7]. But one could use the divergence theorem and conclude erroneously that this integral must always vanish, where V is the volume enclosed by the surface Γ:

$$\oint_{\Gamma} \Omega_n(\mathbf{k}) d\mathbf{S} = \int_V \nabla_{\mathbf{k}}(\Omega_n(\mathbf{k})) dV = \int_V \nabla_{\mathbf{k}}(\nabla_{\mathbf{k}} \times A_n(\mathbf{k})) dV = \int_V 0 dV = 0?? \tag{3.12}$$

This statement is erroneous because the divergence theorem can only be applied to smooth and continuous functions. Although we could try to find a choice of gauge to be smooth and continuous everywhere in the surface, there are some cases where it is impossible to find such a gauge, thereby the Chern number for that manifold will be non-zero. We present briefly a case where the manifold has a singularity, which is a spinor on the magnetic unit sphere[8]. In this system the eigenstates can be represented as,

$$|\uparrow_{\hat{\mathbf{n}}}\rangle = \begin{pmatrix} \cos(\theta/2) \\ \sin(\theta/2) e^{i\varphi} \end{pmatrix}$$

where (θ, φ) are the polar and azimuthal angles of $\hat{\mathbf{n}}$. A gauge choice is implicit in this representation, which makes $|\uparrow_{\hat{\mathbf{n}}}\rangle$ smooth and continuous everywhere, except of a singularity at $\theta = \pi$, where the eigenstate takes different values depending on the azimuthal angle φ: $|\uparrow_{-\hat{\mathbf{z}}}\rangle = \begin{pmatrix} 0 \\ e^{i\varphi} \end{pmatrix}$. Thus it exists a vortex-like singularity in the south pole. We could try to avoid this singularity multiplying a phase $e^{-i\varphi}$ to the eigenvector, which is another valid gauge described by,

$$|\uparrow_{\hat{\mathbf{n}}}\rangle = \begin{pmatrix} \cos(\theta/2) e^{-i\varphi} \\ \sin(\theta/2) \end{pmatrix}$$

but this gauge simply moves the singularity to the north pole ($\theta = 0$). Indeed, there is no possible choice of gauge that is smooth and continuous everywhere in the unit sphere. In such a case, we say that the presence of a non-zero Chern number presents a topological obstruction to the construction of a globally smooth gauge.

[7] When we consider that λ is the reciprocal vector $\mathbf{k}$ a closed path in the reciprocal space describes precisely a two dimensional surface.

[8] The system is described by the Hamiltonian: $H = -\gamma \mathbf{B} \cdot \mathbf{S} = -\left(\frac{\gamma \hbar B}{2}\right) \hat{\mathbf{n}} \cdot \sigma$. Where σ is the vector of the Pauli matrices and $\hat{\mathbf{n}}$ is the direction of $\mathbf{B}$. This example is deeply explained in [2].

We have seen before in the discrete formulation that the Berry phase is gauge invariant when is defined modulo 2π, here we have summarized how each of the Berry quantities transform under a gauge transformation:

Definition	Gauge transformation
$\|u_{n\mathbf{k}}(\mathbf{r})\rangle$	$\|\tilde{u}_{n\mathbf{k}}(\mathbf{r})\rangle \to e^{-i\beta(\mathbf{k})}\|u_{n\mathbf{k}}(\mathbf{r})\rangle$
$A_n(\mathbf{k}) = \langle u_{n\mathbf{k}}(\mathbf{r})\|i\nabla_{\mathbf{k}}\|u_{n\mathbf{k}}(\mathbf{r})\rangle$	$\tilde{A}_n(\mathbf{k}) \to A_n(\mathbf{k}) + \nabla_{\mathbf{k}}\beta(\mathbf{k})$
$\phi_n = \oint_C A_n(\mathbf{k})d\mathbf{k}$	$\tilde{\phi}_n \to \phi_n + 2\pi m \equiv \phi_n \ ; \ m \in \mathbb{Z}$
$\Omega_n(\mathbf{k}) = \nabla_{\mathbf{k}} \times A_n(\mathbf{k})$	$\tilde{\Omega}_n(\mathbf{k}) \to \Omega_n(\mathbf{k})$
$C = \frac{1}{2\pi}\iint_{\partial C}\Omega_n(\mathbf{k})d\mathbf{S}$	$\tilde{C} \to C$

Table 3.1: Gauge transformations of Berry quantities.

Chapter 4

Group Theory

Using Group Theory it is possible to determine the behaviour of a band structure just by looking to the symmetries of a crystal. But first of all, we need to introduce some basic concepts of Group Theory:

Let G be a set of elements which has a defined operation denoted as $\circ$, and satisfies these axioms:

Identity: exists an element(e) that for each $g \in G$ fulfils: $e \circ g = g \circ e = g$.

Inverse: for each element $g \in G$ exists its inverse which fulfils: $g^{-1} \circ g = g \circ g^{-1} = e$.

Closure: if $g_1, g_2 \in G$ then their product also belongs to G : $g_1 \circ g_2 \in G$[1].

Associativity: for all $g_1, g_2, g_3 \in G$: $(g_1 \circ g_2) \circ g_3 = g_1 \circ (g_2 \circ g_3)$.

For further information and demonstrations about the definitions and theorems that will be explained consult [7].

4.1 From site-symmetry to band representation

In this appendix we will deduce how the orbitals transform under the symmetries of the crystal, and give some definitions regarding band representations. First of all, if we consider n_q orbitals on site $\mathbf{q}$ they can be described by a set of Wannier functions[2] $W_{i1}(\mathbf{r})$, where $i = 1, ..., n_q$. Now we shall define the orbit of a Wyckoff position:

Definition: The set of symmetry operations that leave $\mathbf{q}$ invariant is called the site-symmetry group of $\mathbf{q}$, and is denoted $G_{\mathbf{q}} \equiv \{g | g\mathbf{q} = \mathbf{q}\} \subset G$.

Definition: Any two sites whose site-symmetry group are conjugate are said to lie in the same Wyckoff position. Given a site in the Wyckoff position, the number os sites in its orbit[3] that lie in a single unit cell defines the multiplicity of the position.

Definition: A site-symmetry group is non-maximal if exists a finite group $H \neq G_{\mathbf{q}}$, such that $G_{\mathbf{q}} \subset H \subset G$. Then a site-symmetry group that is not non-maximal is maximal. And we say a position $\mathbf{q}$ is maximal when $G_{\mathbf{q}}$ is maximal.

Similarly to the orbital of a Wyckoff position, we define the Wannier functions localized in different Wyckoff positions as $W_{i\alpha}(\mathbf{r}) = g_\alpha W_{i1}(\mathbf{r}) = W_{i1}(g_\alpha^{-1}\mathbf{r})$. For each $g \in G_{\mathbf{q}}$, the functions transform as:

$$gW_{i1}(\mathbf{r}) = [\rho(g)]_{ji} W_{j1}(\mathbf{r}) \tag{4.1}$$

[1] In general $g_1 \circ g_2 \neq g_2 \circ g_1$, equality only occurs in abelian groups.

[2] Wannier functions are a set of orthogonal functions, widely used in Solid State Physics to determine how localized the orbitals are.

[3] The orbit of a Wyckoff position is the set of sites generated by applying operations that are not in the site-symmetry group, so we label those sites by $\mathbf{q}_\alpha \equiv g_\alpha \mathbf{q}_1$, where $\alpha = 1, ..., n$ and $\mathbf{q}_1 \equiv \mathbf{q}$. This group is called the coset representative $G_{\mathbf{q}_\alpha}$.

The Wannier functions localized in other unit cells are defined by $\{E|\mathbf{t}_\mu\}W_{i\alpha}(\mathbf{r}) = W_{i\alpha}(\mathbf{r}-\mathbf{t}_\mu)$, where $\mathbf{t}_\mu$ is a Bravais lattice vector. Hence we have $n \times n_q \times N$ Wannier functions, where $N \to \infty$ and n is the multiplicity of the Wyckoff position. In order to reduce the $n \times n_q \times N$ basis for a finite $n \times n_q$ basis we define the Fourier transformed Wannier functions, which are labelled by $\mathbf{k}$'s residing in the First Brillouin Zone:

$$a_{i\alpha}(\mathbf{k},\mathbf{r}) = \sum_\mu e^{i\mathbf{k}\cdot\mathbf{t}_\mu} W_{i\alpha}(\mathbf{r}-\mathbf{t}_\mu) \tag{4.2}$$

Definition: The band representation ρ_G, induced from n_q-dimensional representation ρ, of the site-symmetry group $G_\mathbf{q}$, of a particular point $\mathbf{q}$ whose orbit contains the sites $\{\mathbf{q}_\alpha \equiv g_\alpha \mathbf{q}\}$ in the unit cell, for the operation $h = \{R|\mathbf{t}\} \in G$, is defined by the action

$$\begin{aligned}
\rho_G(h)a_{i\alpha}(\mathbf{k},\mathbf{r}) &\equiv \rho_G(h)\sum_\mu e^{i\mathbf{k}\cdot\mathbf{t}_\mu} W_{i\alpha}(\mathbf{r}-\mathbf{t}_\mu) \\
&= \sum_\mu e^{i\mathbf{k}\cdot\mathbf{t}_\mu}[\rho(g)]_{ji} W_{j\beta}(\mathbf{r}-\mathbf{t}_\mu-\mathbf{t}_{\beta\alpha}) \\
&= e^{-i(R\mathbf{k})\cdot\mathbf{t}_{\beta\alpha}}[\rho(g)]_{ji}\sum_\mu e^{i(R\mathbf{k})\cdot(R\mathbf{t}_\mu+\mathbf{t}_{\beta\alpha})} W_{j\beta}(\mathbf{r}-\mathbf{t}_\mu-\mathbf{t}_{\beta\alpha}) \\
&= e^{-i(R\mathbf{k})\cdot\mathbf{t}_{\beta\alpha}}[\rho(g)]_{ji} a_{j\beta}(R\mathbf{k},\mathbf{r})
\end{aligned} \tag{4.3}$$

Where in the second step we have used the result (B1) of Appendix B in [1], $\rho_G(h)W_{i\alpha}(\mathbf{r}-\mathbf{t}_\mu) = [\rho(g)]_{ji}W_{j\beta}(\mathbf{r}-R\mathbf{t}_\mu-\mathbf{t}_{\beta\alpha})$, on the third step we have used the fact that R is orthogonal. In the final result Einstein's notation is assumed, where $j = 1, ..., n_q$ and the index β is determined by the unique coset of G that contains hg_α:

$$hg_\alpha = \{E|\mathbf{t}_{\beta\alpha}\}g_\beta g \tag{4.4}$$

Where $g \in G_\mathbf{q}$, g_β are coset representatives[4], and $\mathbf{t}_{\beta\alpha}$ must be a Bravais lattice vector, which is obtained from the previous equation $\mathbf{t}_{\beta\alpha} = h\mathbf{q}_\alpha - \mathbf{q}_\beta$.

The matrix form of $\rho_G(h)$ consists of infinitely many $(n\cdot n_q)\times(n\cdot n_q)$ blocks, which are labelled by $\mathbf{k}$ in the first BZ, so we denote each block by $\rho^\mathbf{k}_G(h)_{j\beta,i\alpha} \equiv e^{-i(R\mathbf{k})\cdot\mathbf{t}_{\beta\alpha}}\rho_{ji}(g_\beta^{-1}\{E|-\mathbf{t}_{\beta\alpha}\}hg_\alpha)$. Now if we want to compute how the band representation is composed with the irreps of a specific k-point, $\sigma^\mathbf{k}_i$, we have to do the subduction of ρ_G onto $G_\mathbf{k}$, where $G_\mathbf{k}$ is the little group[5] of $\mathbf{k}$. The subduction is denoted by $\rho_G \downarrow G_\mathbf{k}$, in order to know the decomposition we need to calculate the characters of the representation:

$$\chi^\mathbf{k}_G(h) \equiv \sum_\alpha e^{-i(R\mathbf{k})\cdot\mathbf{t}_{\alpha\alpha}}\chi[\rho(g_\beta^{-1}\{E|-\mathbf{t}_{\beta\alpha}\}hg_\alpha)] \tag{4.5}$$

[4]The coset representatives are the symmetry operations that transform a Wyckoff position into the other sites in its orbit, up to a lattice vector, thus $g_\beta\mathbf{q} \equiv \mathbf{q}_\beta$.

[5]$G_\mathbf{k}$ is defined by $G_\mathbf{k} = \{h = \{R|\mathbf{t}|R\mathbf{k} \equiv \mathbf{k}, h \in G\}$.Where the equality is up to a reciprocal lattice vector.

When the characters are calculated, we can obtain the decomposition with the *Magic Formula* (A.5) explained in Appendix A, thus we can find how many times each $\sigma_i^{\mathbf{k}}$ appears in $\rho_G \downarrow G_{\mathbf{k}}$:

$$(\rho \uparrow G) \downarrow G_{\mathbf{k}} \cong \bigoplus_i m_i^{\mathbf{k}} \sigma_i^{\mathbf{k}} \tag{4.6}$$

Once we have established how to decompose a band representation, now we can define topological bands.

Definition: A set of bands are in the *atomic limit* of a space group if they can be induced from localized Wannier functions consistent with the crystalline symmetry of that space group. Otherwise, they are *topological*. Thus, *topological bands* must be groups of bands that satisfy the crystal symmetry in momentum space, but do not transform as a band representation.

In this work, we will not compute this operations manually. Instead, we will use the program *vasp2trace* and the tool 'Check Topological Mat' [5] in order to determine the topology of the crystals. For a more detailed explanation on how this procedure is performed see Appendix B.

4.2 Enforced Semimetals

In order to understand what enforced semimetals are we need to introduce the concept of compatibility relations. A set of Bloch wavefunctions that obey the crystal symmetry will, at each point in the BZ, transform as a sum of irreps of the little group at that point. For instance, given a high-symmetry line ($\mathbf{q}_0$) that connects two high-symmetry points ($\mathbf{q}$ and $\mathbf{q}'$), the little group of the line ($G_{\mathbf{q}_0}$) is the intersection of the little groups of both points $G_{\mathbf{q}_0} = G_{\mathbf{q}} \cap G_{\mathbf{q}'}$. It follows that each irrep that appears in the band decomposition at the point can be subduced to a sum of irreps that appear on the line, therefore the irreps that appear along the line are completely determined by the irreps in the point. This decomposition is known as the compatibility relation between a high-symmetry point and line.

Moreover, this relations are remarkably useful to determine how bands are connected throughout the BZ. For instance, following the general example from before, with two high-symmetry points ($\mathbf{q}$ and $\mathbf{q}'$) that are connect with the line $\mathbf{q}_0$, if it is determined that the band representations from each point along the line decompose as $\rho^1_{\mathbf{q}} \to \Delta_1$ $\rho^1_{\mathbf{q}'} \to \Delta_1$; $\rho^2_{\mathbf{q}} \to \Delta_2$ $\rho^2_{\mathbf{q}'} \to \Delta_2$, then when the crystal is imposed to an adiabatic deformation, if the symmetry of the crystal is conserved during this process, the compatibility relation ensures that $\rho^1_{\mathbf{q}}$ will be connected to $\rho^1_{\mathbf{q}'}$ the same as $\rho^2_{\mathbf{q}}$ will be connected to $\rho^2_{\mathbf{q}'}$.

Notice that this relation does not guarantee that there will not be a crossing along the line $\mathbf{q}_0$, if exists a crossing along the line that is not a consequence of a symmetry it is denominated as an accidental crossing. This accidental crossing may occur when $E_2(\mathbf{q}) < E_1(\mathbf{q})$; $E_2(\mathbf{q}') < E_1(\mathbf{q}')$, like in figure 4.1b. However, depending on the Hamiltonian it could exist a configuration like 4.1a, where there is no crossing, but when a deformation is applied, the energies of both bands could interchange in one point, while conserving their compatibility relation, as a consequence a crossing would occur between the two points without a doubt 4.1c. Thus this crossing is demanded by the symmetry of the crystal, and when this happens we say the material is an enforced semimetal.

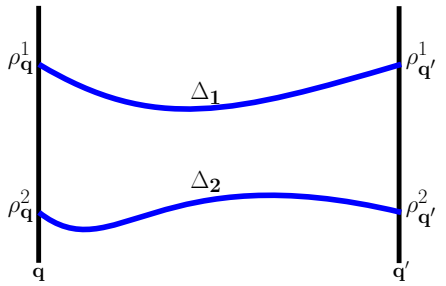

(a) No crossing

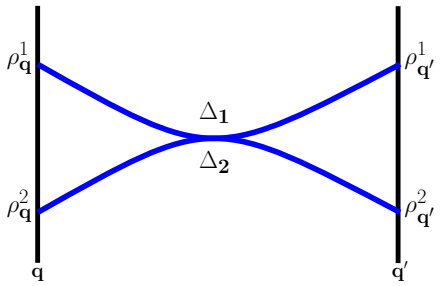

(b) Accidental crossing

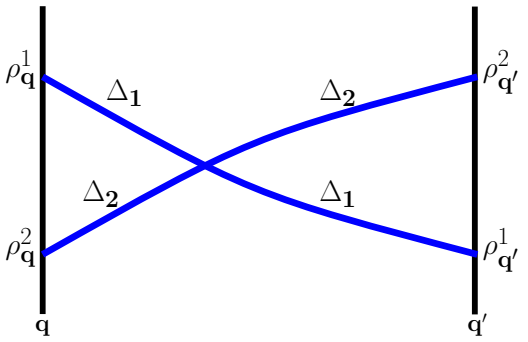

(c) Enforced crossing

Figure 4.1: Three different band structures with the same compatibility relation. (a) $E_2(\mathbf{q}) < E_1(\mathbf{q})$; $E_2(\mathbf{q}') < E_1(\mathbf{q}')$ is satisfied but there is not a crossing protected by symmetry along the line, (b) there is a crossing that is not protected by symmetry thus it is accidental, (c) the energies in $\mathbf{q}'$ are swapped so there must exist a crossing which is protected by symmetry.

Chapter 5

First principles calculations

Many *abinitio* programs have been developed to perform different calculations, such as ionic relaxation, band structure or phonon and dynamics. Vienna Abinitio Simulation Package (VASP) is a software developed by G. Kresse et al. [8, 9, 10, 11], which solves the many-body Schrodinger equations, using approximations such as DFT (Density Functional Theory) or the Hartree-Fock approximation.

We will need this program for our particular case, because we aim to study a crystal with 24 atoms and 224 electrons in the unit cell. Thus in order to obtain results as accurate as possible we will need to rely on First principles calculations, and VASP is a perfect candidate to fulfil our goal.

In this chapter we introduce the principles in which VASP is based, but without going into too much detail about the algorithms it uses to do the calculations. Although VASP is programmed to reduce time and memory usage while performing an accurate calculation, *ab initio* algorithms are so time and memory expensive that we will have to use a supercomputer in order to get results in a plausible time frame. The one we are using is the supercomputer Atlas, provided by the DIPC (Donostia International Physics Center).

5.1 Density Functional Theory

DFT is used to solve a many-body problem, concretely the ground state of a crystal. Considering Hartree atomic units we assume that $e = m_e = \hbar = 1$, so a general Hamiltonian for a system consistent of N electrons (N being of the order of Avogadro's number $\sim 10^{23}$) is,

$$\mathbf{H} = -\frac{1}{2}\sum_i \nabla_i^2 - \frac{1}{2M_I}\sum_I \nabla_I^2 + \frac{1}{2}\sum_{i\neq j}\frac{1}{|\mathbf{r}_i - \mathbf{r}_j|} - \sum_{i,I}\frac{Z_I}{|\mathbf{r}_i - \mathbf{R}_I|} + \frac{1}{2}\sum_{I\neq J}\frac{Z_I Z_J}{|\mathbf{R}_I - \mathbf{R}_J|} \tag{5.1}$$

where the contribution from the left to right are the kinetic energy of all electrons, the kinetic energy of the nucleus, the Coulomb interaction between electrons, the interaction between nucleus and electrons, and the nuclei-nuclei interaction. Due to its complexity this Hamiltonian is straight up intractable, thus some approximation are considered in order to simplify the problem.

The first one is to consider the nuclei frozen, ergo, they do not move, therefore their kinetic energy contribution is totally nullified and their positions ($\mathbf{R}_I$) are considered parameters. Then the last contribution in equation 5.1 is constant with respect to the electron positions ($\mathbf{r}_i$), so we can ignore it. This approximation is called the Born-Oppenheimer or the adiabatic approximation.

Nonetheless, even removing nuclei variables, there are still N electrons to consider in the problem, so a rough way to calculate the ground state is to construct a wave function[1] which is antisymmetric to permutations[2] (5.2), and minimize the Hamiltonian over the wave function with the constrains of normalization. Thus, Lagrange multipliers method is necessary for this task (5.3).

$$\psi(\mathbf{r}_1\sigma_1, ..., \mathbf{r}_N\sigma_N) = \frac{1}{\sqrt{N!}} \begin{vmatrix} \psi_1(\mathbf{r}_1\sigma_1) & \dots & \psi_1(\mathbf{r}_N\sigma_N) \\ \vdots & \ddots & \vdots \\ \psi_N(\mathbf{r}_1\sigma_1) & \dots & \psi_N(\mathbf{r}_N\sigma_N) \end{vmatrix} \tag{5.2}$$

$$F[\{\psi_i(\mathbf{r}_j\sigma_j); \varepsilon_i\}] = \langle \mathbf{H} \rangle_\psi - \sum_i \varepsilon_i(\langle \psi_i | \psi_i \rangle - 1) \;\Rightarrow\; \frac{\delta F}{\delta \varepsilon_i} = 0 \;;\; \frac{\delta F}{\delta \overline{\psi}_i} = 0 \tag{5.3}$$

With this method we get the well known Hartree Fock equations 5.4, where the third term is the screening contribution of the other electrons and the fourth term is the exchange correlation energy, which is a purely Quantum contribution to the Hamiltonian. However, those ε_i must not be confused with the eigenenergies of the crystal, actually, Koopman's theorem proves that those values the ionisation energies but with the opposite sign.

$$\begin{aligned} -\frac{1}{2}\nabla^2\psi_i(\mathbf{r}\sigma) + U_{ion}(\mathbf{r})\psi_i(\mathbf{r}\sigma) + \sum_{j,\sigma'} \int d\mathbf{r}' \frac{|\psi_j(\mathbf{r}'\sigma')|^2}{|\mathbf{r}-\mathbf{r}'|}\psi_i(\mathbf{r}\sigma) \\ - \sum_{j,\sigma'} \int d\mathbf{r}' \frac{\delta_{\sigma,\sigma'}}{|\mathbf{r}-\mathbf{r}'|}\overline{\psi}_j(\mathbf{r}'\sigma')\psi_i(\mathbf{r}'\sigma)\psi_j(\mathbf{r}\sigma') = \varepsilon_i\psi_i(\mathbf{r}\sigma) \end{aligned} \tag{5.4}$$

On the other side, DFT ensures that the ground state energy of a crystal and the external potential are totally determined by the ground state electronic density [12]. It is founded on these two theorems:

Theorem 1: For any system of interacting particles in an external potential $V_{ext}(\mathbf{r})$, the potential is determined uniquely (except for a constant), by the ground state particle density $n_0(\mathbf{r})$.

Theorem 2: A universal functional for the energy $E[n]$ in terms of the density $n(\mathbf{r})$ can be defined, valid for any external potential $V_{ext}(\mathbf{r})$. The previous mentioned ground state particle density minimizes that energy.

In other words, we can write the electronic Hamiltonian as a functional of the electronic density n($\mathbf{r}$), and calculate its ground state energy by using the functional derivative and equalising it to zero:

$$\mathbf{H} = E[n(\mathbf{r})] \;;\; \frac{\delta E}{\delta n(\mathbf{r})}\Big|_{n_0(\mathbf{r})} = 0 \;;\; E[n_0(\mathbf{r})] = E_0 \tag{5.5}$$

[1] σ means a spin state.
[2] This wave function is also known as Slater determinant.

5.2 The Kohn-Sham method

Now that we know the paramount of DFT, we need to know the form of the Hamiltonian in function of the density. First of all, we can decompose the energy functional as down below.

$$E[n] = T[n] + \int V_{ext}(\mathbf{r})n(\mathbf{r})d\mathbf{r} + E_H[n] + E_{XC}[n] \tag{5.6}$$

The Kohn-Sham method assumes that the kinetic energy has the form of the free electron kinetic energy (5.7), otherwise there is no way to know its form. The next term is the external potential created by the nuclei, followed by the Hartree energy, which represents the electron-electron Coulomb interaction (5.8). Finally, the last term is the Exchange-Correlation energy, it has an unknown form, and different estimations are considered to approximate it, which we will discuss them in section 5.4.

$$T[n] = \frac{3}{10}(3\pi^2)^{\frac{2}{3}} \int [n(\mathbf{r})]^{5/3} d\mathbf{r} \tag{5.7}$$

$$E_H[n] = \frac{1}{2} \int \int \frac{n(\mathbf{r})n(\mathbf{r}')}{|\mathbf{r}\text{-}\mathbf{r}'|} d\mathbf{r}d\mathbf{r}' \tag{5.8}$$

It is important to specify that the density is calculated with equation 5.9, $\phi_i(\mathbf{r})$ being the wave function of the i-th electron, and the wave function of the system is a Slater determinant, which is constructed as the equation 5.2.

$$n(\mathbf{r}) = \sum_{i=1}^{N} |\phi_i(\mathbf{r})|^2 \tag{5.9}$$

Now we minimize the energy functional with respect to the density, although it is equivalent to derive respect to the wave function $\overline{\phi}_i(\mathbf{r})$, because they fulfil the relation $\delta n(\mathbf{r}) = \delta\overline{\phi}_i(\mathbf{r})\phi_i(\mathbf{r})$. To do such minimization we use again the Lagrange multipliers method as before in equation 5.3, but replacing $\langle \mathbf{H} \rangle_\psi$ by $E[n]$. With this procedure we get:

$$\mathbf{H}_{eff}\phi_i(\mathbf{r}) = \Big(-\frac{1}{2}\nabla^2 + V_{ext}(\mathbf{r}) + V_H(\mathbf{r}) + V_{XC}(\mathbf{r}) \Big)\phi_i(\mathbf{r}) = \varepsilon_i\phi_i(\mathbf{r}) \tag{5.10}$$

Here $V_H(\mathbf{r}) = \frac{1}{2}\int d\mathbf{r}' \frac{n(\mathbf{r}')}{|\mathbf{r}-\mathbf{r}'|}$ is the Hartree potential, and $V_{XC} = \frac{\delta E_{XC}[n]}{\delta n(\mathbf{r})}$ is the Exchange-Correlation potential[3]. Now, the last step is to solve the equations 5.10, but they are a set of coupled equations, because the effective Hamiltonian depends on the density $n(\mathbf{r})$, which depends in all the wave functions $\phi_i(\mathbf{r})$. Thus, this must be solved with an iterative method, which we will explain in the next section.

[3]The sum of all the potential is called the Kohn-Sham method : $V_s(\mathbf{r}) \equiv V_{ext}(\mathbf{r}) + V_H(\mathbf{r}) + V_{XC}(\mathbf{r})$

5.3 Self Consistent Calculation

Continuing with the Kohn-Sham method, we have arrived to a set of coupled equations with the form 5.11. These equations can be solved with iterative algorithms, in this section we will explain briefly the Self Consistent Calculation (SCC), which can be easily visualised in the figure 5.1.

$$\mathbf{H}_{eff}[n(\mathbf{r}) = \sum_{i=1}^{N} |\phi_i(\mathbf{r})|^2]\phi_i(\mathbf{r}) = \varepsilon_i\phi_i(\mathbf{r}) \tag{5.11}$$

In this diagram δ is an energy threshold which determines the accuracy of the ground state energy we get from this algorithm, this is calculated with the difference between the energy related to the density of the previous iteration and the new one: $|E[n_{new}] - E[n_{previous}]| = |\Delta E|$.

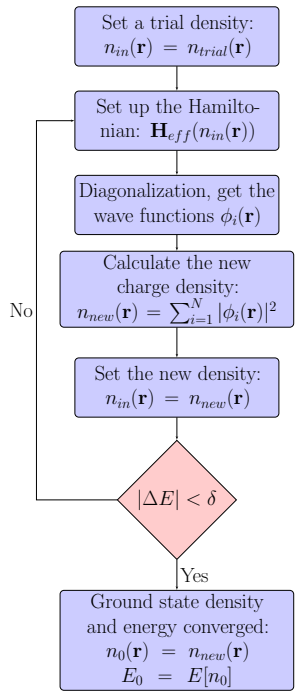

Figure 5.1: Self Consistent Calculation algorithm diagram.

The calculation starts with a trial density ($n_{trial}(\mathbf{r})$), then the effective Hamiltonian is calculated[4]. When the Hamiltonian is diagonalized the wave functions are obtained, therefore the density can be recalculated, which will give a new value of the energy ($E[n_{new}]$). Finally, the difference between the new and the previous energy is calculated, and it is checked if that difference is smaller than the given threshold, if it is bigger then we go back to the second step with the new density, otherwise we have concluded the calculations and we know the ground state density and energy of the system.

[4]As DFT states this Hamiltonian depends on the electric density, but there is one term which has unknown form, the Exchange correlation potential, two approximations to estimate its form are discussed in the following section.

5.4 Pseudopotentials

Pseudopotentials are widely used in solid state calculations [13], the main idea is to replace the exact potential (if known) by an approximated one, which is commonly obtained from phenomenological data. In this way, instead of calculating a really difficult Hamiltonian's (H_{exact}) spectrum, we get as close as possible to the exact one, simplifying lot of calculations because the eigenfunctions and eigenvectors of H_{PP} are more easily accessible through efficient computer codes rather than calculating in the traditional way with H_{exact}, at least at the region of interest.

It is well known that the valence electrons are the most important in a chemical process, while core electrons remain unaware, therefore, core electron's contribution to the potential are commonly not taken into account[5]. Core states are localized in the vicinity of the nucleus, whereas the valence states must oscillate in order to keep the orthogonality with the core eigenfunctions. This involves large kinetic energy around the core region, which is roughly cancelled by the Coulomb interaction. In 1934 Hans G.A. Hellmann replaced this effects with a pseudopotential, which was repulsive in the core region and kept the electrons away from the core.

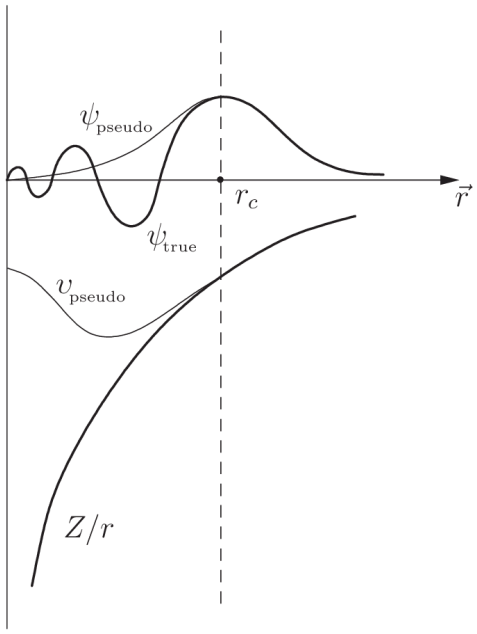

Figure 5.2: Here we can understand graphically the main intention of the pseudopotential method. Instead of having a divergent potential (the Coulomb potential V), which produces oscillating eigenfunctions, we replace it with a potential (V_{pseudo}) that converges in $r = 0$ and tends to equal V when $r > r_c$, r_c being the cut-off radius which determines our range of interest. We choose the pseudopotential to get eigenfunctions which have no nodes and change smoothly. Ref: [14].

In general, pseudopotentials are angular momentum dependent, thus it can be expressed as:

$$V_{ps}(\mathbf{r}) = \sum_{\infty}^{l=0} \sum_{l}^{m=-l} v_l(r) \overline{Y}_l^m(\theta, \phi) Y_l^m(\theta, \phi) \tag{5.12}$$

[5]This is known as Frozen-core approximation.

However, when Spin Orbit Coupling (SOC) is considered, angular momentum $\mathbf{L}$ is not be conserved, therefore l is not a good quantum number anymore. What is conserved is the total angular momentum $\mathbf{J} = \mathbf{L} + \mathbf{S}$, and due to the electron having spin $= \frac{1}{2}$ the values of J are $J = L \pm \frac{1}{2}$. Regularly, this pseudopotentials are constructed using both values of J, nevertheless, we are not going into much detail in this topic, and a general way to consider this interaction is to add this relativistic effect with the form:

$$V_{ps}^{SOC}(\mathbf{r}) = \sum_{l=0}^{\infty} \sum_{l}^{m=-l} v_l^{SOC} \mathbf{L} \cdot \mathbf{S}\, \overline{Y}_l^m(\theta, \phi) Y_l^m(\theta, \phi) \tag{5.13}$$

Hence, the total pseudopotential would be:

$$V_{ps}^{total}(\mathbf{r}) = V_{ps}(\mathbf{r}) + V_{ps}^{SOC}(\mathbf{r}) \tag{5.14}$$

On top of that, the wave function now are spinors, with one component for each spin value $S = \pm\frac{1}{2}$:

$$\phi_i(\mathbf{r}) = \begin{pmatrix} \phi_{\uparrow i}(\mathbf{r}) \\ \phi_{\downarrow i}(\mathbf{r}) \end{pmatrix} \tag{5.15}$$

As a result, the new normalization condition has the form:

$$\int d\mathbf{r} |\phi_{\uparrow i}(\mathbf{r})|^2 + |\phi_{\downarrow i}(\mathbf{r})|^2 = 1 \tag{5.16}$$

The main issue when using DFT is to know the form of the Exchange-Correlation energy, thus, many approximations have been developed, among them we will discuss the Local Density Approximation (LDA) and the Generalized Gradient Approximation (GGA).

5.4.1 Local Density Approximation (LDA):

In this approximation it is assumed that the ε_{XC} has at each $\mathbf{r}$ point the value it would have a uniform electron gas with density $n(\mathbf{r})$. If we decompose the X-C energy density, the exchange energy density of a uniform electron gas has the form 5.18:

$$\varepsilon_{XC}(n) = \varepsilon_X(n) + \varepsilon_C(n) \tag{5.17}$$

$$\varepsilon_X^{unif}(n) = -\frac{3}{4}\Big(\frac{3}{\pi}\Big)^{1/3} n^{1/3} \tag{5.18}$$

Even so, we can not know the exact form of correlation energy density, but it can be numerically calculated using accurate quantum Monte Carlo method. Here we show a parametrized estimation of the uniform electron gas correlation energy density:

$$\varepsilon_C^{unif}(n) \approx \begin{cases} A\ln(r_s) + B + Cr_s\ln(r_s) + \mathcal{O}(r_s) & \text{if High-density: } r_s \longrightarrow 0 \\ \frac{a}{r_s} + \frac{b}{r_s^{3/2}} + \mathcal{O}(\frac{1}{r_s^2}) & \text{if Low-density: } r_s \longrightarrow \infty \end{cases} \tag{5.19}$$

Where r_s is the radius each electron would occupy in the uniform electron gas with a density n: $r_s = \left(\frac{3}{4\pi n}\right)^{1/3}$. However, the most used parametrization is the one Perdew and Wang presented in 1992 [15]:

$$\varepsilon_C^{unif}(n) = 2A(1+\alpha r_s)\ln\Big[1 + \frac{1}{2A(\beta_1 r_s^{1/2} + \beta_2 r_s + \beta_3 r_s^{3/2} + \beta_4 r_s^{p+1})}\Big] \tag{5.20}$$

Where the fitting parameter values can be found in the reference.

5.4.2 Generalized Gradient Approximation (GGA):

The first step after the LDA approximation was to consider that the X-C energy depends also on the gradient of the density, the Gradient-Expansion Approximation[6] included a new term in the X-C energy as we can see in 5.21:

$$E_{XC}^{GEA}(n) = \int \varepsilon_{XC}^{unif} n(\mathbf{r}) \Big[1 + C\Big(\frac{\nabla n}{2k_F(\mathbf{r})n(\mathbf{r})}\Big)^2\Big] d\mathbf{r} \ ; \ k_F(\mathbf{r}) = (3\pi^2 n(\mathbf{r}))^{1/3} \tag{5.21}$$

Nonetheless, GEA was later confirmed to be worse than LDA for real systems. Thus, they generalized that idea defining the Generalized-Gradient Approximation, which states: $E_{XC}^{GGA}(n) = \int f(n(\mathbf{r}), \nabla n(\mathbf{r}) d\mathbf{r}$, where f is an unknown function that needs to be estimated.

Perdew et al. published a GGA implementation in 1996 [16], called Perdew-Burke-Ernzerhof (PBE):

$$\begin{gathered}
E_X^{GGA} = \int n(\mathbf{r}) \varepsilon_X^{unif}(n) F_X^{PBE}(s) d\mathbf{r} \qquad E_C^{GGA} = \int n(\mathbf{r})(\varepsilon_C^{unif}(n) + H^{PBE}(r_s, t)) d\mathbf{r} \\
F_X^P BE(s) = 1 + \gamma - \frac{\gamma}{1+\mu s^2} \qquad H^{PBE}(r_s, t) = \frac{\beta^2}{2\alpha} \ln\Big[1 + \frac{2\alpha}{\beta} \frac{t^2 + At^4}{1 + At^2 + A^2 t^4}\Big] \\
s = \frac{|\nabla n|}{2k_F(\mathbf{r})n(\mathbf{r})} \qquad A = \frac{2\alpha}{\beta e^{-2\alpha\varepsilon_c^{unif}(n)/\beta^2} - 1} \\
t = \frac{|\nabla n|}{2k_s(\mathbf{r})n(\mathbf{r})} \ ; \ k_s = \Big(\frac{4k_F}{\pi}\Big)^{1/2}
\end{gathered} \tag{5.22}$$

5.5 Bloch wavefunctions

In order to construct a crystal a unit cell is needed, where the atoms reside, and three lattice vectors which determines the Bravais lattice[7], which we will refer to as direct space. A general lattice vector would have the form:

$$\mathbf{R} = n_1\mathbf{a}_1 + n_2\mathbf{a}_2 + n_3\mathbf{a}_3 \ ; \ n_i \in \mathbb{Z} \tag{5.23}$$

As the crystal has a translational symmetry[8] so does the Hamiltonian of the system:

$$\hat{T}_{\mathbf{R}} \hat{H}(\mathbf{r}) = \hat{H}(\mathbf{r} + \mathbf{R}) \hat{T}_{\mathbf{R}} = \hat{H}(\mathbf{r}) \hat{T}_{\mathbf{R}} \ \Rightarrow [\hat{T}_{\mathbf{R}}, \hat{H}(\mathbf{r})] = 0 \tag{5.24}$$

This symmetry is fundamental for the Band Structure theory and calculation [17], because it provides really important information about the Hamiltonian eigenfunctions. It is a well known result that if two operator commute (5.24) they can be simultaneously diagonalized, which in other terms means that they share the eigenfunctions. What is more, we know the form of the eigenfunctions of the translation operator:

$$\hat{T}_{\mathbf{R}} e^{i\mathbf{kr}} = e^{i\mathbf{k}(\mathbf{r}+\mathbf{R})} = e^{i\mathbf{kR}} e^{i\mathbf{kr}} \tag{5.25}$$

So the eigenvalue is $e^{i\mathbf{kR}}$, where the vector $\mathbf{k}$ is the label of the eigenfunction. This can be generalized, if the eigenfunction is multiplied by a periodic function in $\mathbf{R}$ then it will also be an eigenfunction of the operator $\hat{T}_{\mathbf{R}}$:

$$\psi_{\mathbf{k}}(\mathbf{r}) = e^{i\mathbf{kr}} u_{\mathbf{k}}(\mathbf{r}) \ ; \ u_{\mathbf{k}}(\mathbf{r} + \mathbf{R}) = u_{\mathbf{k}}(\mathbf{r}) \Rightarrow \hat{T}_{\mathbf{R}} \psi_{\mathbf{k}}(\mathbf{r}) = e^{i\mathbf{kR}} \psi_{\mathbf{k}}(\mathbf{r}) \tag{5.26}$$

[6] This method would be equivalent to take more terms in a Taylor series approximation.
[7] A Bravais lattice is an array of discrete points created by discrete translations.
[8] The discrete translation operator $\hat{T}_{\mathbf{R}}$ leaves the crystal invariant.

Consequently, the eigenfunctions of the Hamiltonian have the form[9], this are called the Bloch wave functions (5.26). On the other hand, we could ask ourselves if different $\mathbf{k}$ labels could have the same eigenvalue:

$$e^{i\mathbf{kR}} = e^{i\mathbf{k'R}} \Rightarrow e^{i(\mathbf{k}-\mathbf{k'})\mathbf{R}} = 1 \Rightarrow (\mathbf{k}-\mathbf{k'})\cdot\mathbf{R} \equiv \mathbf{G}\cdot\mathbf{R} = 2\pi n \ ; \ n \in \mathbb{Z} \tag{5.27}$$

Thus, a vector $\mathbf{G}$ can be defined which satisfy the equation 5.27:

$$\mathbf{G} = m_1\mathbf{b}_1 + m_2\mathbf{b}_2 + m_3\mathbf{b}_3 \ ; \ m_i \in \mathbb{Z} \tag{5.28}$$

Where the basis vectors $\{\mathbf{b}_i\}$ are the ones who fulfil $\mathbf{a}_i \cdot \mathbf{b}_j = 2\pi\delta_{i,j}$. Remarkably, the form in which $\mathbf{G}$ is constructed is equal to the form 5.23, therefore $\mathbf{G}$ describes another Bravais lattice, which is called the reciprocal lattice (or reciprocal space). In general, if the crystal was infinite a lattice vector $\mathbf{k}$ could take any continuous value, but real crystals are not infinite, thus it is assumed the has N unit cells[10]. Considering Born-von Karman periodic boundary conditions $\mathbf{k}$ can only take this quasi-continuous values[11]:

$$\mathbf{k} = k_1\mathbf{b}_1 + k_2\mathbf{b}_2 + k_3\mathbf{b}_3 \ ; \ k_i = \frac{n_i}{N_i} \ ; \ n_i \in [0, N_i - 1] \tag{5.29}$$

The next obvious step is to express the Hamiltonian eigenfunctions in terms of plane waves[12]:

$$\begin{aligned} u_{n,\mathbf{k}}(\mathbf{r}) &= \sum_{\mathbf{G}} C_{n,\mathbf{k}}(\mathbf{G}) e^{i\mathbf{Gr}} \\ \psi_{n,\mathbf{k}}(\mathbf{r}) &= \sum_{\mathbf{G}} C_{n,\mathbf{k}}(\mathbf{G}) e^{i(\mathbf{k}+\mathbf{G})\mathbf{r}} \end{aligned} \tag{5.30}$$

VASP works with plane waves, however, we need to truncate the values of $\mathbf{G}$ for numerical reasons, thus a parameter called *cutoff energy* can be specified on the calculations, which determines how many terms will be taken into account (5.31). Increasing this value results in more accurate calculations, even so more computation time will be needed.

$$\frac{(\mathbf{k}+\mathbf{G})^2}{2} \leq E_{cutoff} \tag{5.31}$$

Finally, we can calculate the eigenvalues of the Hamiltonian:

$$\hat{H}\psi_{n,\mathbf{k}}(\mathbf{r}) = \varepsilon_n(\mathbf{k})\psi_{n,\mathbf{k}}(\mathbf{r}) \tag{5.32}$$

The set of energies $\{\varepsilon_n(\mathbf{k})\}$ are the so called bands, and they are functions of the reciprocal lattice vector. In order to plot those bands in two dimensions a specific path is chosen in the reciprocal space, this path consists of high-symmetry lines inside or in the boundaries of the first Brillouin Zone. The first Brillouin Zone, also called simply Brillouin Zone, is the Wigner-Seitz cell of the reciprocal space, which is the set of points (describing a volume, a zone) that are closer to the origin (Γ point) than to any other point in the Bravais lattice. The shape of the BZ depend on the Bravais lattice of the direct space, leading to different K-paths, in section 6.3 the BZ and K-path for our material will be shown.

[9] But we have to consider different energy levels (n), so the equation 5.26 can be generalized: $\psi_{n,\mathbf{k}}(\mathbf{r}) = e^{i\mathbf{kr}}u_{n,\mathbf{k}}(\mathbf{r})$

[10] It is more accurate to say that the crystal has $\{N_1, N_2, N_3\}$ cells for each direction$\{\mathbf{a}_1, \mathbf{a}_2, \mathbf{a}_3\}$, then the total number of cells would be $N = N_1N_2N_3$.

[11] As a consequence of $\mathbf{k'} \equiv \mathbf{k} + \mathbf{G}$ we have stated that n_i is bounded, but it could take any integral value.

[12] It can be proven that a periodic function's expression has the form 5.30:

$$u_{n,\mathbf{k}}(\mathbf{r}) = u_{n,\mathbf{k}}(\mathbf{r}+\mathbf{R}) = \textstyle\sum_{\mathbf{k'}} C_{n,\mathbf{k}}(\mathbf{k'}) e^{i\mathbf{k'}(\mathbf{r}+\mathbf{R})} = u_{n,\mathbf{k}}(\mathbf{r}) e^{i\mathbf{k'R}} \Rightarrow e^{i\mathbf{k'R}} = 1 \Rightarrow \mathbf{k'} \in \mathbf{G}$$

Chapter 6

Material features

Before applying pressure to our materials we will discuss their different physical properties. In this chapter we present their crystalline structure and symmetries, then we see the interatomic distances as well as the energy per atom provided by VASP, and finally we compare the band structures for Ag_3AuSe_2 with LDA and GGA approximations along with considering spin-orbit coupling or not.

6.1 Crystalline structure and symmetries

Ag_3AuSe_2's space group is $I4_132(214)$, as well as Ag_3Te_2Au's, which is non-symmorphic[1]. Its primitive cell has a rhombohedral structure, with angles $\alpha{=}\beta{=}\gamma{=}109.4712°$. However, relaxation has been made with the cubic cell due to simplicity. Furthermore, in order to later calculate the Electronic Band Structure, the primitive unit cell was needed, which can be constructed[2] from the cubic one (6.1b).

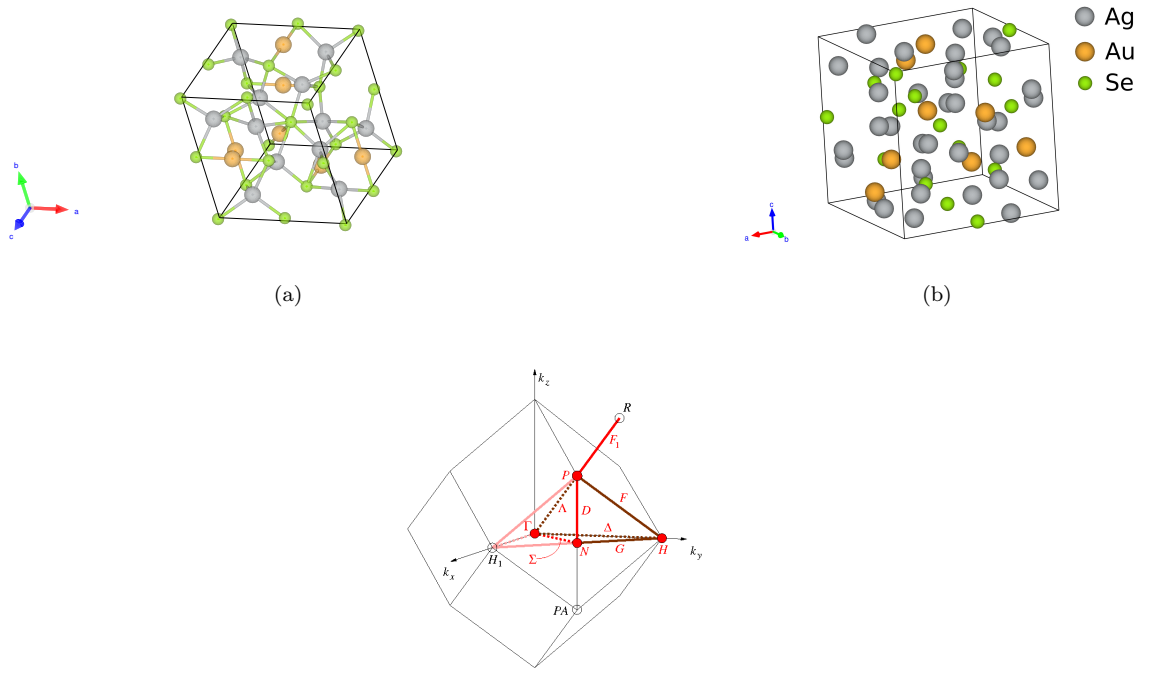

(a) (b)

(c)

Figure 6.1: (a)Ag_3AuSe_2's primitive cell obtained with VESTA [18], Ag_3Te_2Au's is not shown because it has basically the same form, they only differ in the lattice parameter and the interatomic distances. (b) Ag_3AuSe_2's conventional (cubic) cell. (c) First Brillouin Zone of the group 214 and the high symmetry points. K-path described with red lines: $\Gamma - H - N - \Gamma - P - H|P - N$.

[1] A non-symmorphic group is a group which has fractional lattice vector translations.

[2] This can be achieved with a program named *phonopy*, which takes the cubic structure as input and returns the primitive cell in the file PPOSCAR.

The group 214 consists of 6 symmetry generators (Table 6.1) and other 3 pure translations, one for each lattice vector. As previously stated, the group is non-symmorphic, because its symmetry operations imply partial translations, for example operation number 2.

No.	Symmetry operation(Seitz symbols)
1	$\{E\|0\}$
2	$\{2_{001}\|1/2\ 0\ 1/2\}$
3	$\{2_{010}\|0\ 1/2\ 1/2\}$
4	$\{3^{+}_{111}\|0\}$
5	$\{2_{110}\|3/4\ 1/4\ 1/4\}$
6	$\{1\|1/2\ 1/2\ 1/2\}$

Table 6.1: 214 space group's symmetry operations. On the left we have the symmetry operator and on the right the coordinates of the translation in terms of lattice vectors.

Any material's structure can be found in the Materials Project website [19], where we have gathered all this information.

6.2 Atomic parameters

In this section we only focus on Ag_3AuSe_2, because as we have stated before, both material's structures are practically identical. Furthermore, there is another reason why we focus only on this material, but this is due to the results in section 7.3.

In Table 6.2, different lattice parameters are shown, depending on which approximation has been used in order to calculate them[3], including the experimental value, as well as the total energy per atom, considering different approximations.

Lattice parameter	LDA(Error%)	GGA(Error%)	Experimental
a (Å)	9.75(6)	10.14(2)	10.38

(a) Lattice parameters

Energy per atom	LDA NSOC	LDA SOC	GGA NSOC	GGA SOC
$E_{tot}(eV/atom)$	-4.01	-4.06	-3.15	-3.20

(b) Total energy per atom

Table 6.2: (a) Lattice parameter of the crystal for a body centered cubic cell, errors with respect the experimental value are given in percentages. (b) Energy per atom when the structure is relaxed.

We see in 6.2 that the energy per atom is greater (in magnitude) when LDA approximation is considered, this is due to more repulsive core-valence contribution to the exchange-correlation energy in GGA. Precisely, as a consequence of this repulsion the lattice parameter is greater with GGA, leading to larger interatomic distances, these distances can be observed in Table 6.3.

[3]For LDA or GGA, the lattice parameters do not differ if SOC is considered or not.

VASP also provides interatomic distances, which differ if they are calculated with LDA or GGA pseudopotentials, those distances are presented in Table 6.3. Notice LDA calculations give smaller distances than GGA.

Ag-Se	2.68	2.68	2.83	2.83
Au-Se	2.48	2.48		
Ag-Ag	2.95	2.95	3.03	3.04
Au-Au	3.45	3.45	3.45	
Ag-Au	2.95	2.95		

(a) Interatomic distances in Å(LDA NSOC)

Ag-Se	2.69	2.69	2.82	2.82
Au-Se	2.48	2.48		
Ag-Ag	2.94	2.94	3.04	3.04
Au-Au	3.45	3.45	3.45	
Ag-Au	2.93	2.93		

(b) Interatomic distances in Å(LDA SOC)

Ag-Se	2.79	2.79	2.92	2.92
Au-Se	2.50	2.50		
Ag-Ag	3.08	3.08	3.13	3.13
Au-Au	3.58	3.58	3.58	
Ag-Au	3.08	3.08		

(c) Interatomic distances in Å(GGA NSOC)

Ag-Se	2.79	2.79	2.92	2.92
Au-Se	2.50	2.50		
Ag-Ag	3.08	3.08	3.13	3.13
Au-Au	3.58	3.58	3.58	
Ag-Au	3.08	3.08		

(d) Interatomic distances in Å(GGA SOC)

Table 6.3: Interatomic distances between nearest neighbours

First of all, we notice that the average distance between the atoms is ~ 3Å, in addition, Au-Se are the nearest so we could expect a stronger interaction among those atoms. What is more, we can see that interatomic distances do not depend on SOC, since with LDA the difference vary only in the second decimal and with GGA there is no difference at all. However, those distances do change when considering LDA or GGA, it is easy to see that LDA gives smaller distances, therefore we can understand why total energy (6.2) is bigger (in magnitude), it is due to a higher contribution of the Coulomb interaction.

6.3 Band Structure

In this section we calculate the electronic band structure with different pseudopotentials and including or excluding Spin-Orbit Coupling. Band Structures with different approximations are given in Figure 6.2. Because the energy depends on the three coordinates of $\mathbf{k}$ (5.5) , in order to plot the energy in 2 dimensions we need to define a K-path, this path is already established for every cell structure, which we can see in the Figure 6.1, it is constructed by high symmetry lines in the Brillouin Zone[4] and can be demonstrated that this path has all the information about the energy structure. A Monkhorst-Pack k-point grid of $(7 \times 7 \times 7)$ has been used for reciprocal space integration and a 500 eV energy cutoff (5.31) of the plane-wave expansion.

[4]The first Brillouin Zone is the Wigner-Seitz cell of the reciprocal space.

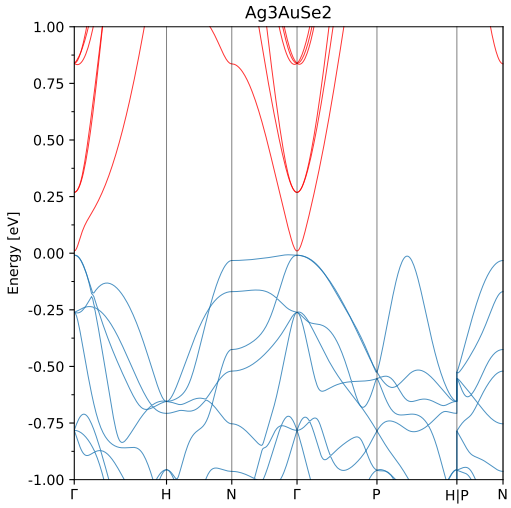

(a) Band structure NSOC and LDA

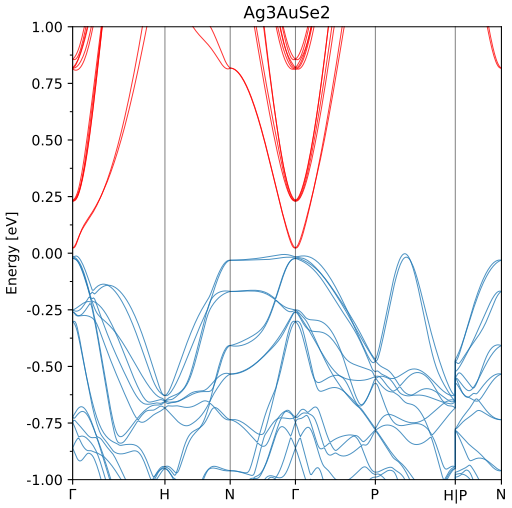

(b) Band structure SOC and LDA

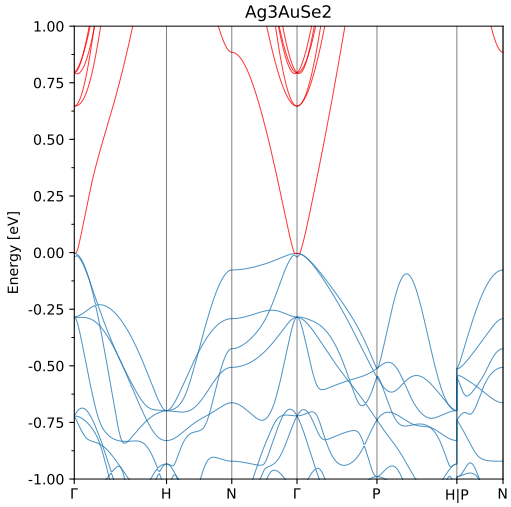

(c) Band structure NSOC and GGA

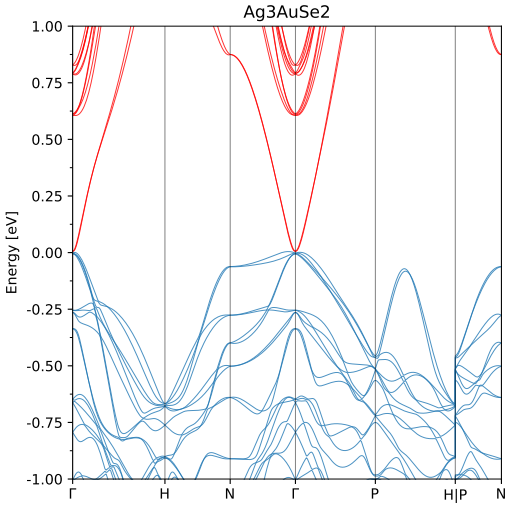

(d) Band structure SOC and GGA

Figure 6.2: Band Structure within the range $[-1eV, 1eV]$ having the Fermi level at the origin. The red bands represent empty (conduction) bands. The BS (c) coincides reasonably with the one Materials Project website provides, since this one is also calculated without SOC and with GGA.

When SOC is considered the bands split, as it is expected the spin contribution breaks the degeneracy of the bands. The clearest example is the crossing above the Fermi level at point H, before SOC is considered there is a three-fold crossing of doubly degenerate bands[5], this crossing splits into two crossings, a two-fold and a four-fold of non degenerate bands.

We do not see many differences with the BS using LDA or GGA whatsoever, but the main contrast is the band gap, with LDA there is a very small one, but with the GGA there is no gap. However, this deviation is not very relevant, considering the experimental value of the gap is $\sim 0.9eV$, thus both approximations fail when it comes to calculate the band gap. This is a well known problem of the DFT method, because it performs poorly when computing band gaps.

For the sake of simplicity, as we have seen in 5.4, GGA is theoretically more accurate than LDA because it includes density's gradient on the calculations[6], therefore we will proceed our next calculations with only GGA approximation.

[5] When spin is omitted all bands are doubly degenerate: $H \neq H(\sigma) \Rightarrow H\psi_{\pm}(\mathbf{k}) = \varepsilon(\mathbf{k})\psi_{\pm}(\mathbf{k})$.

[6] It would be analogous to consider higher terms of Taylor's series of a function, meaning we want to be more accurate.

Chapter 7

Results

As mentioned in Chapter 1 our aim is to cause a phase transition of the both crystals from trivial insulators to topological, by applying pressure, positive and negative pressures will be applied, even though the negative pressures are physically impossible to achieve they will serve for academical purposes.

7.1 Seeking a topological transition

In order to apply pressure, we have manually altered lattice parameters of each crystal, by means of lattice parameter percentages, thus the new parameters are calculated by $a' = a_0(1+\gamma)$, where $\gamma = \frac{\Delta a}{a_0} \in [-8\%, ..., 0\%, ..., 7\%]$. Therefore, the negative values of γ correspond to compression (positive pressure) and the positives to expansion (negative pressure, physically infeasible). Furthermore, as the lattice parameter of both crystals are of order $a_0 \sim 10$Å, then lattice parameters are varied with steps of order $\Delta a \sim 0.1$Å.

Afterwards, we have performed a relaxation calculation, this way we ensure the crystal is in equilibrium. We make an atomic relaxation while fixing the lattice parameters, this way the volume and shape remain intact and thus the symmetry is not changed. This calculation also returns the internal energy (U) of the crystal as well as the pressure (P), which their relation is given by:

$$P = -\frac{\partial U}{\partial V} \tag{7.1}$$

Where V is the volume of the unit cell, this relation is fulfilled when $T \sim 0K$, so it is expected a good agreement between the pressure given by VASP calculation and the numerical one obtained with 7.1, because VASP performs those calculations with low temperature. Both results for each material are presented in the following Figure.

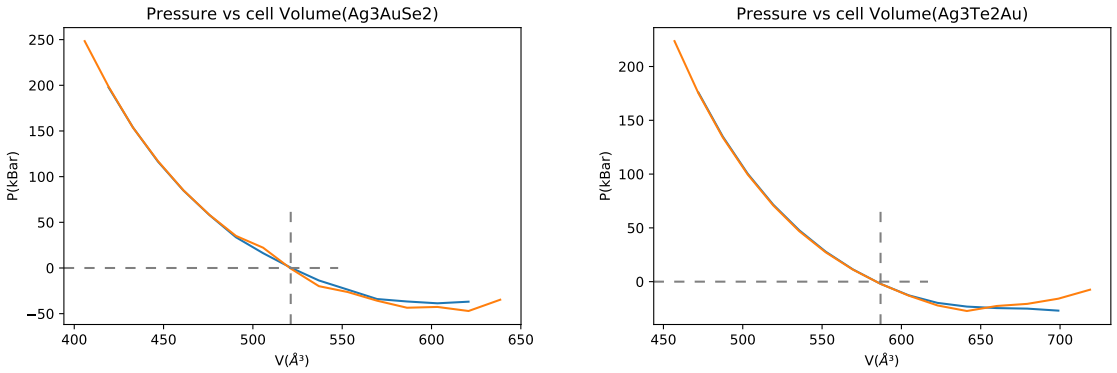

Figure 7.1: Graphics showing the pressure (kBar) of both materials as a function of the unit cell volume (Å^3), where the orange line is the pressure returned by the relaxation calculation and the blue one is obtained from 7.1, for numerical reasons the first and last point was not computed for the blue line. The dashed lines indicate the equilibrium volume of the cell, where the pressure must be 0.

These graphics demonstrate that 7.1 is satisfied, as the "experimental" and numerical data coincide in a wide range, although they differ a little when negative pressure is applied.

After applying pressure the band structure can be calculated, the band structures for $P = 0$ have already been presented in the previous chapter 6. Here we present the BS for both materials when $\gamma = -8\%$ and $\gamma = 7\%$.

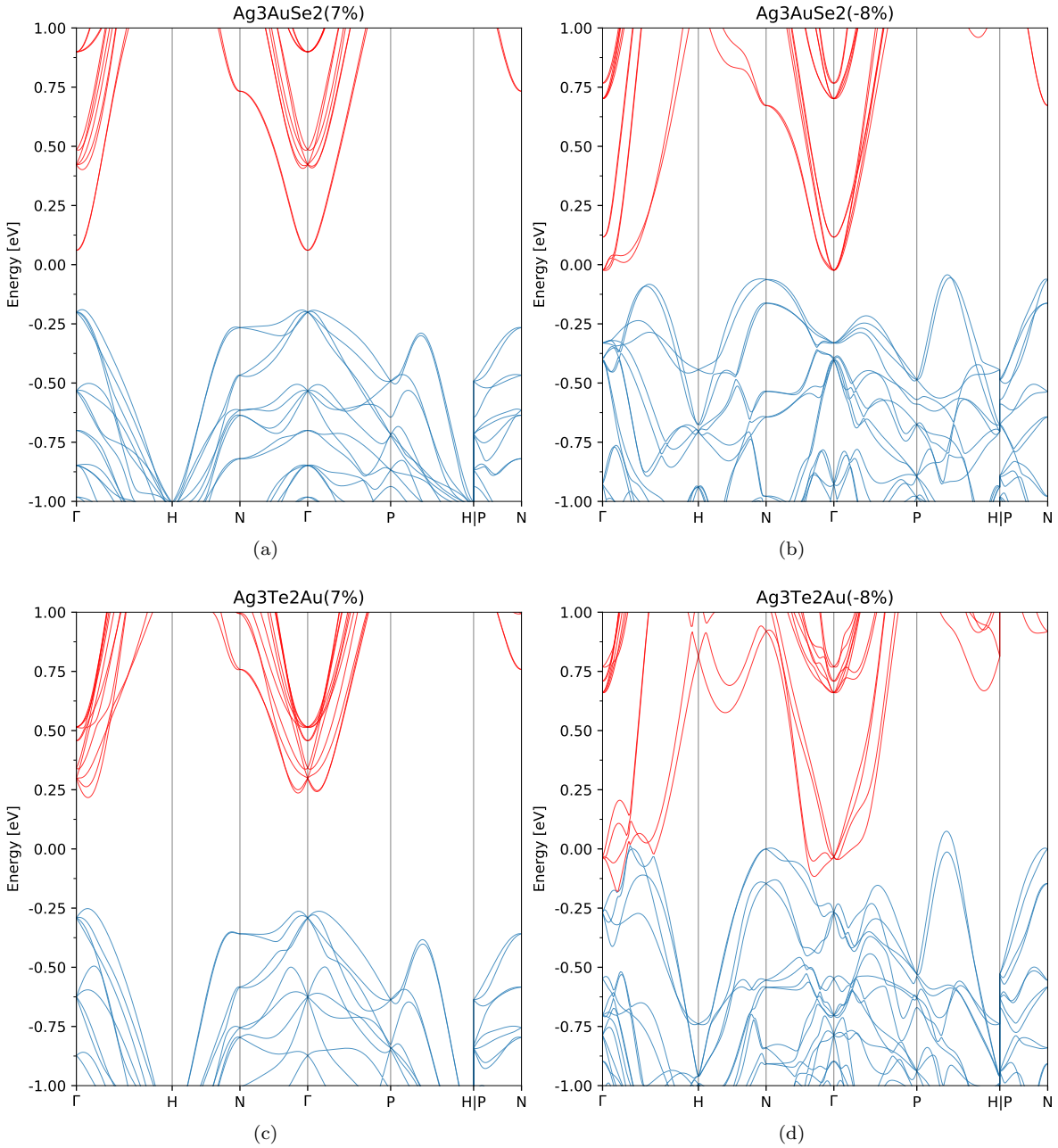

Figure 7.2: BS for Ag_3AuSe_2 and Ag_3Te_2Au with the maximum positive and negative pressure applied. It is not possible to see with these two examples but Ag_3AuSe_2's gap decreases when positive pressure tends to zero and start increasing when negative pressure increases. Unlike Ag_3Te_2Au's case, where the gap increases when pressure decreases, even when pressure is negative.

Even though it is of interest to see how the BS transform when pressure is applied, the main interest is to see if these materials exhibit a phase transition into topological insulators. This phase transitions are studied with Vasp2trace in the next section.

7.2 Vasp2trace analysis

As explained in Appendix B, we have computed *trace.txt* files for each BS with different pressures and attached to Dgenpos [5], obtaining whether the material is topological or not. Ag_3Te_2Au has a phase transition from trivial insulator into an Enforced Semimetal with Fermi Degeneracy (ESFD) when $1\% \leq \gamma \leq 5\%$, and Ag_3AuSe_2 is also an ESFD when $1\% \leq \gamma$. This phase transition arises when an irrep inversion is produced, fortunately Dgenpos provides the irreps that lie below the chemical potential, so in the Table and Figure below this phenomena is visible for Ag_3AuSe_2.

Trivial			ESFM		
N	Γ	P	N	Γ	P
$\overline{N}_5(2)$	$\overline{\Gamma}_8(4)$	$\overline{P}_7(3)$	$\overline{N}_5(2)$	$\overline{\Gamma}_8(4)$	$\overline{P}_7(3)$
$\overline{N}_5(2)$	$\overline{\Gamma}_8(4)$	$\overline{P}_5(1)$	$\overline{N}_5(2)$	$\overline{\Gamma}_6(2)$	$\overline{P}_7(3)$
$\overline{N}_5(2)$	$\overline{\Gamma}_6(2)$	$\overline{P}_7(3)$	$\overline{N}_5(2)$	$\overline{\Gamma}_8(4)$	$\overline{P}_5(1)$
$\overline{N}_5(2)$	$\overline{\Gamma}_8(4)$	$\overline{P}_4(1)$	$\overline{N}_5(2)$	$\overline{\Gamma}_6(2)$	$\overline{P}_4(1)$
$\overline{N}_5(2)$	$\overline{\Gamma}_6(2)$	$\overline{P}_7(3)$	$\overline{N}_5(2)$	$\overline{\Gamma}_8(4)$	$\overline{P}_7(3)$

Table 7.1: Irreducible representations below the Fermi level at N, Γ and P for Ag_3AuSe_2. Where the number between the brackets indicates the dimension of each irrep. Notice that the irreps in N are always the same and do not change in the phase transition, whereas in Γ and P those irreps are changed. The lines over the representations indicate that they are double valued, because spinful states are considered.

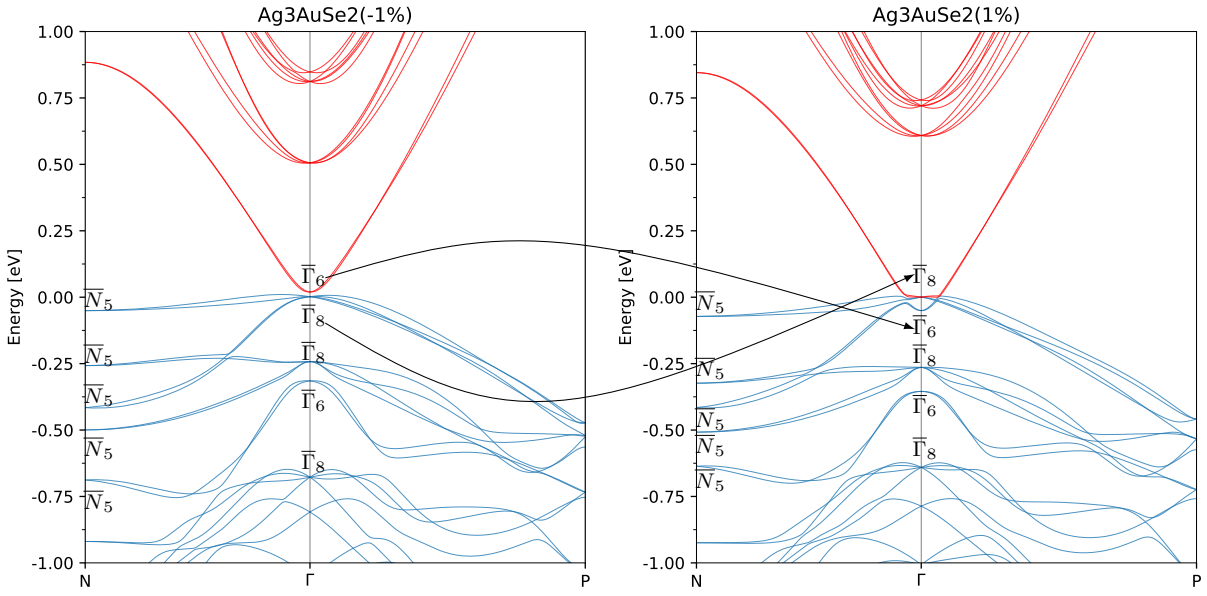

Figure 7.3: In concordance with 7.1, a band inversion is observed in this Figure. The twofold band in Γ above the Fermi level ($\overline{\Gamma}_6$) in the trivial case swaps with the fourfold band ($\overline{\Gamma}_8$).

In the paper [20] is proved that non-symmorphic groups lead to enforced band crossing, which is a property of the enforced semimetals. Thus we have shown that varying the lattice parameter of Ag_3AuSe_2, an ESFD has arisen with group $I4_132(214)$ which is indeed non-symmorphic, and produces the band inversion present in table above.

7.3 Possible Dark Matter detector

Even though a topological transition has not been achieved, a particular BS of Ag_3AuSe_2 may be of interest, which is the one with $\gamma = -2\%$.

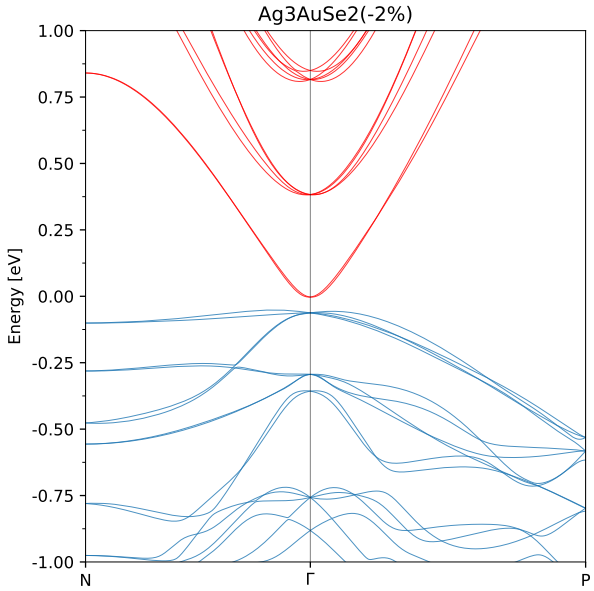

Figure 7.4: Here the BS is plotted only in the k-path $N - \Gamma - P$ because the dispersion around the Γ is crucial for the purpose of detecting dark matter.

In this case, a small gap of $\sim meV$ in the Γ point, as well as the linear dispersion of the conduction bands and the valence bands being quite plane around the Γ point makes this a good candidate for a Dark matter detector. What's more, a paper has been published about the utility of this material for the DM detection [21], where it has been studied following the methodology presented in [22]. On this paper [21] an effective model has been calculated, which is used to derive the optical conductivity from the band structure.

In order to deduce the form of the effective model group theory has been used. This can be fulfilled obtaining the irreps of the valence and conduction bands, and determining which bands contribute the most for those bands. The latter can be plotted with a program written in *Python*, *pyband_color.py*, which uses the data from the OUTCAR and the PROCAR[1]. This permits to see in a coloured map of the BS to visualize each orbitals weights, also allowing to perform this analysis for each atom in the unit cell. Here we show two examples, one for a negligible contribution and another which has a high weight in certain region of the BS.

[1]The OUTCAR contains the values of the energy bands, whereas the PROCAR contains the weights.

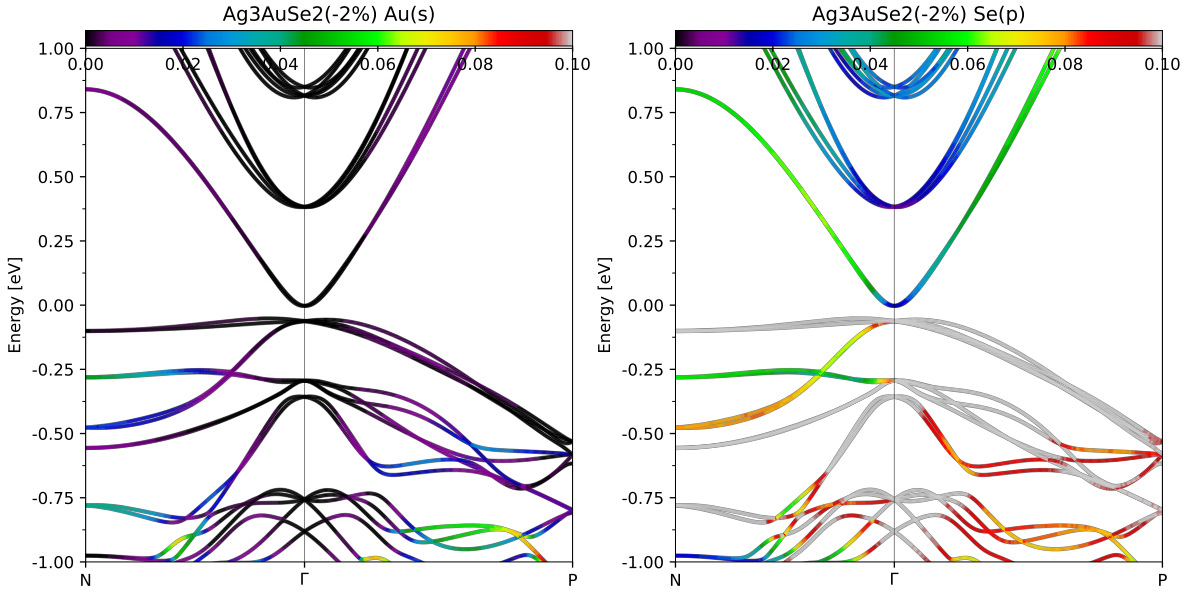

(a) (b)

Figure 7.5: Orbital contributions for certain orbitals in certain atoms. (a) Low weights for s orbitals in gold. (b) Appreciable contribution for the valence bands for p orbitals in selenium, being the grey colour the maximum.

Analysing every orbital for each type of atom in the cell, we conclude that these orbitals are the most relevant in the BS: s orbitals in silver and selenium, p orbitals in selenium and d orbitals in silver and gold. With this information (also with the irreps of bands) a $\mathbf{k}\cdot\mathbf{p}$ Hamiltonian describing the band structure near the Γ point has been developed in *Mathematica*. This general form consists in a 6×6 matrix:

$$H(\mathbf{k}) = \begin{pmatrix} H_{2band}(\mathbf{k},\alpha,v_F) + \Delta 1_{2\times 2} & H_{cp}(\mathbf{k},\delta) \\ H_{cp}(\mathbf{k},\delta)^\dagger & H_{4band}(\mathbf{k},v_F^1,v_F^2) - \Delta 1_{4\times 4} \end{pmatrix}, \tag{7.2}$$

Where the 2×2 block H_{2band} describes the two conduction bands, the 4×4 block H_{4band} to the four valence bands, H_{cp} parametrises the overlap of these bands and the parameter Δ determines the direct band gap width. The exact form of each block and the values for the fitting parameters can be checked in Appendix C.

These parameters are fitted to the BS obtained with VASP for hydrostatic pressures with compressions $\gamma = -1\%, -2\%, -3\%$. In the three cases the band structure exhibits a fourfold node below the Fermi level and a Weyl node above it, separated by a gap that varies with the pressure. The interband contribution to the conductivity tensor $\sigma_{\mu\nu}$, where $\mu,\nu = x,y,z$, can be calculated using standard linear response theory as the real part of[2]:

$$\sigma_{\mu\nu}(w) = \frac{ie^2}{wV}\sum_{m\neq n}\frac{\langle n|\, j_\mu\, |m\rangle\langle m|\, j_\nu\, |n\rangle}{\epsilon_n - \epsilon_m + \hbar w + i\delta}(n_F(\epsilon_n) - n_F(\epsilon_m)) \tag{7.3}$$

[2]This equation is a generalization of the one presented in Appendix A of the paper [22]. As we are considering optical transitions $\mathbf{q}\sim 0$ and for simplicity we do not write the integral over $\mathbf{k}$ in the first Brillouin Zone.

Where $j_\mu = \frac{1}{\hbar}\partial_{k_\mu} H$ is the current operator defined by the Hamiltonian, e is the charge of the electron, V is the volume, $|n\rangle$ and E_n are an eigenstate and the corresponding eigenvalue of the Hamiltonian respectively, δ is an infinitesimal broadening; $\epsilon_n = E_n - \mu$, where μ is the chemical potential and n_F is the Fermi distribution, which depends on E_n, μ and the inverse temperature $\beta = 1/k_B T$ in units of Boltzmann constant k_B. With this equation σ_{xx} has been computed using the effective model considering valence to conduction band transitions and valence interband transitions.

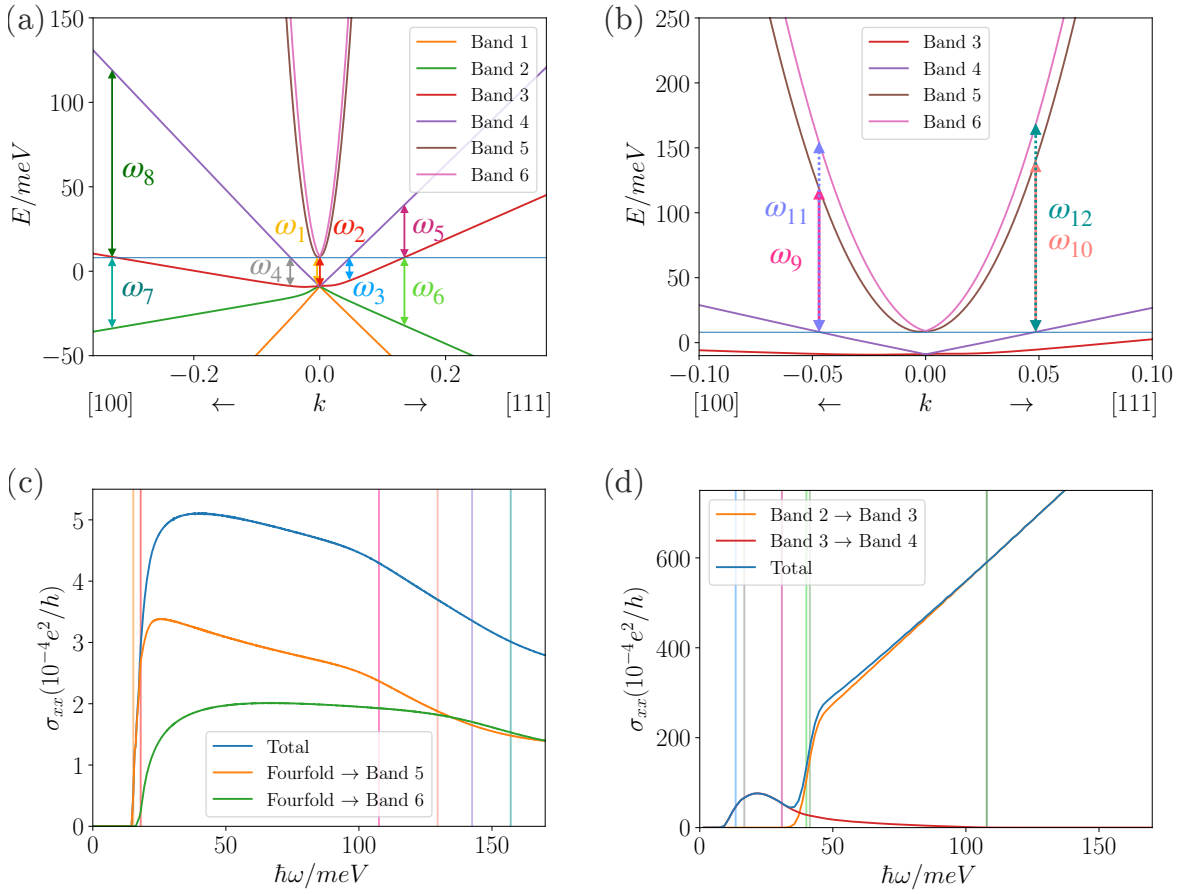

Figure 7.6: Optical conductivity of the low energy $\mathbf{k}\cdot\mathbf{p}$ model of Ag_3AuSe_2 under 1% hydrostatic pressure. (a) and (b) show the same band structure within two different energy windows, together with the relevant frequencies for optical transitions (colored vertical arrows) and the chemical potential (blue horizontal line). The bands are labelled with numbers from 1 to 6 from bottom (orange band) to top (pink band). Figures (c) and (d) show the optical conductivity corresponding to valence to conduction band transitions (c) and interband transitions between the valence bands (d), with $\beta = 1/k_B T = 2\times10^3$.

The feasibility for dark matter detection is determined by four main requirements [22]: i) If one is to detect dark matter with keV mass, it is necessary a band gap of order $\sim meV$. As we have argued, Ag_3AuSe_2's band gap with the pressures we have applied reaches the range of meV, satisfying the first point. ii) Fermi velocity must be smaller than the largest possible dark matter velocity, $v_{max} \sim 10^{-3}c$. Indeed, from C.1 we know that all the Fermi velocities are $v_F \sim 10^{-4}c < v_{max}$, so it satisfies the second point. iii) There must be small photon screening at energies close to the energy deposition range. The imaginary part of the dielectric tensor determines the absorption of the material, and is related to the optical conductivity by $\epsilon = 1 + i\sigma/w$. In Figure 7.6 (c) we see that the optical conductivity tends to a constant value except for the 3% case, where it grows linearly ($\sigma \propto w$) with a small slope, resulting in a dielectric constant that renders a small in-medium polarization for the photon, thus satisfying the third point. iv) Finally, a dark matter detector must be sensible to a small number of counts per year, for which the target material must be grown as large and pure as possible. Currently we do not know if Ag_3AuSe_2 satisfies this condition.

Chapter 8

Conclusions

In this work, we have studied how the electronic band structure of Ag_3AuSe_2 and Ag_3Te_2Au change when pressure is applied. It was observed that the gap for Te[1] did not close for any applied pressure, furthermore, its transition to ESFD occurs with negative pressure, thus it is not physically feasible to obtain that phase transition. On the other hand, for Se, for some values of negative pressure the gap disappears ($1\% \leq \gamma \leq 4\%$), and it also has a transition to ESFD with negative pressure, which is produced by an irrep inversion, as visualized in 7.1. For none of the pressures applied a topological transition is achieved, consequently, our search for a topological material has not been successful.

Nevertheless, another interesting result was obtained from this research. When a pressure with $\gamma = -2\%$ was applied to Se, its band dispersion around Γ seemed to be appropriate to use as a detector for Dark Matter. In order to study profoundly its optical properties an effective model was constructed[2], and the results derived from that calculus were published in [21]. For a proper analysis experimental results will be needed in the future, because our *ab initio* calculations could be erroneous, or rather a small difference between theoretical and the experimental BS could lead to very different behaviour of the material. For example, a wrong estimation of the band gap could make our material's gap to be too large to detect DM, as stated in 7.3 we need a band gap of $\sim meV$, and one of the main flaws of DFT is precisely the estimation of the band gap.

Another line of study could be to consider magnetic interactions within the crystal, applying an external magnetic field. This is a tricky one, because when magnetism is considered time-reversal symmetry takes an essential role, because spinful particles are not invariant under time-reversal any more. This leads to consider all the spatial symmetries alongside time-reversal (resembling the operation of a full 2π rotation $\overline{E}$ when spinful states are considered). There are 32 point group, which are the groups that have symmetries without any translation, when translations are considered more groups can be constructed, which leave 230 space groups, but when time-reversal is also considered, the magnetic space group contains 1651 symmetry groups in it. Hence when a magnetic field is applied to the crystal, a bunch of new symmetries and representations take part in the group theory, which hinders the calculus. Fortunately, Bilbao Crystallographic Server also provides the representations, Wyckoff positions and many other features of magnetic groups, which helps considerably with a complete examination of any material, though this was not of our concern for our inquiry.

Moreover, other materials similar to Ag_3AuSe_2 can be analysed with the methodology presented in this work, for instance, Ag_3AuS_2 or Ag_3AuSeS. With these material we expect the spin orbit splitting to be smaller, as selenium is heavier than sulfur, and according to the paper [23] in general heavier materials experience larger splitting. Another way to acquire topological matter is to reduce in some way the symmetries of the crystal, this could be accomplished for example adding some iron to $PtSe_2$, which would break the mirror symmetries, as well as for $Fe_{1/4}TaS_2$ in paper [24].

We must remark that group theory was a key element in this work, we have used its tools to analyse if our materials were topological, and it was also used to obtain the general form of the effective model for Se ($\gamma = -2\%$), demonstrating how powerful it is, as mentioned in 2.3. Another crucial tool has been the *ab initio* package VASP, which was used to calculate all BS that were needed in order to develop our research, as well as the wavefunctions for the Vasp2trace analysis.

[1] As both materials difference is just Te or Se, we will use this abbreviation.
[2] As presented in the last section 7.3.

Appendix A

Representations and Characters

Isomorphism: a transformation $[a(e_j) = a_{ij}e_i]$ that admits an inverse transformation $(det(a) \neq 0)$.

Linear representation: a homomorphism (a function that preserves the operations defined on an object) from the group G into the group GL(V). In other words, we associate with each element $s \in G$ an element $\rho(s)$ of GL(V), in such a way[1]:

$$\rho(st) = \rho(s) \cdot \rho(t) \tag{A.1}$$

$$\rho(e) = \mathbb{I} \quad \rho(s^{-1}) = \rho^{-1}(s) \tag{A.2}$$

Similar representations: Let ρ and ρ' be two representations of the same group G in vector space V and V'. We say they are similar if exists a linear isomorphism $\tau : V \longrightarrow V'$ which transforms ρ into ρ'[2]:

$$\tau \cdot \rho(s) = \rho'(s) \cdot \tau \ ; \ for \ \forall s \in G \tag{A.3}$$

Subrepresentations: Let $\rho : G \longrightarrow GL(V)$, and W be a subspace of V. Suppose that W is stable(invariant) under the elements of G($x \in W \Rightarrow \rho(s) \cdot x \in W$). The restriction of ρ to W is then an isomorphism of W onto itself. And $\rho^W : G \longrightarrow GL(W)$ is said to be a subrepresentation of ρ.

Irreducible representations(irreps): $\rho : G \longrightarrow GL(V)$ is irreducible or similar if no subspace of V is stable under G. In other words, V is not the direct sum of irreducible representations, except the trivial decomposition $V = 0 \oplus V$.

Trace("Character"): The trace of a matrix as we know is the sum of all its diagonal components $(Tr(a) = \sum_i^n a_{ii})$, this sum does not depend on the basis we use to represent said matrix, this is a very convenient property, because we do not want our calculations to depend on the basis used, therefore, the traces of the representations will be crucial. The set of traces of a representation(of the matrices $\rho(s)$) is called the character of a representation[3]. It is denoted as χ, being $\chi_\rho(s) = Tr(\rho(s))$ and fulfilling these properties:

- $\chi_\rho(e) = n$; n is the dimension of the vector space V and e the identity of the group G.
- $\chi_\rho(s^{-1}) = \overline{\chi_\rho(s)}$; characters in general are complex numbers.
- $\chi_\rho(tst^{-1}) = \chi_\rho(s)$
- $\chi_\rho(ts) = \chi_\rho(st)$

Proposition: Let $\rho^1 : G \longrightarrow GL(V_1)$ and $\rho^2 : G \longrightarrow GL(V_2)$.

i The character χ of $V_1 \oplus V_2$ is equal to $\chi_1 + \chi_2$.

ii The character of ψ of $V_1 \otimes V_2$ is equal to $\chi_1 \cdot \chi_2$.

[1] In pursuit of simplifying our notation we will assume $s \circ t \equiv st$.

[2] Notice that we represent the product between matrices with $\cdot$, which does not have any relation with the product between two elements of G($\circ$).

[3] It is quite misleading but the name "character" is also used to refer to traces, but strictly it means the set of traces.

Scalar product: A scalar product between characters can be defined. In the future it will be highly important, since key conclusions are derived from properties of this product:

$$(\chi|\psi) = \frac{1}{g}\sum_{t\in G}\chi(t)\overline{\psi(t)} \tag{A.4}$$

Theorem:

i If χ is the character of an irrep then $(\chi|\chi) = 1$. What is more, the latter only is true if and only if the representation is irreducible. This gives a good criteria in order to check if the representation is irreducible or not.

ii If χ and χ' are characters of two non isomorphic irreps then $(\chi|\chi') = 0$.(i.e. χ and χ' are orthogonal)

Theorem: Let V be a lin. rep. of G, with character ψ, and being the decomposition $V = m_1W_1 \oplus ... \oplus m_kW_k$ (k is the number of not equivalent irreps of G). If W_i is an irrep with character χ_i, the multiplicity of said irrep is equal to the scalar product $(\psi|\chi_i)$. This is called the number of times that W_i occurs in V. Furthermore, A.5 equation is called the *Magic formula*, because of its importance knowing how a representation decomposes, computing its character with the characters of the irreps.

$$m_i = (\psi|\chi_i) \tag{A.5}$$

Conjugacy classes: Let $t, t' \in G$, we say that t and t' are conjugate(or belong to the same conjugacy class) if exist $s \in G$ such that $t' = sts^{-1}$. For example, there are three classes[4] in the group $C_{3V} : \{\{E\}, \{C_3^+, C_3^-\}, \{\sigma_{d1}, \sigma_{d2}, \sigma_{d3}\}\}$.

Theorem: The number of non-equivalent irreducible representations for a finite group G(previously denoted as k) is equal to the number of classes in G.

Theorem: The sum of the squares of the dimensions of the non-equivalent irreps of a finite group G is equal to the order of the group(the number of elements in G).

$$\sum_{i=1}^{k} n_i^2 = g \tag{A.6}$$

Double valued representations: When spin is considered ($s = \frac{1}{2}$), then ρ will be a double valued representation, such that a 2π rotation gives a phase $e^{2\pi is} = -1$. Thus other symmetry operations must be taken into account, being $\overline{E}$ the one corresponding to the 2π rotation, which is $-\mathbb{I}$, and the rest being composition of the previous symmetry operations and $\overline{E}$. Computing their characters is as simple as $\chi(t\overline{E}) = \chi(t)\chi(\overline{E})$.

Physically irreducible representations: Time-reversal symmetry is crucial and every physical system must respect that symmetry (when magnetic moments are not considered). If we want to know if a representation is time-reversal invariant, we can compute the Frobenius-Schur indicator, which is defined by:

$$\Phi(\rho) = \frac{1}{g}\sum_{t\in G}\chi(t^2) = \begin{cases} 1, & \rho \textit{ is real} \\ 0, & \rho \textit{ is complex} \\ -1, & \rho \textit{ is pseudoreal} \end{cases}$$

As far as we are concerned, the representations ρ are always double valued, and as it is demonstrated in [1], if ρ is pseudoreal and double valued, then it is time-reversal invariant. However, if it is not invariant, ρ must be paired with its complex conjugate representation in order to have an invariant representation $\rho \oplus \rho^*$.

[4]Conjugacy class is usually shorten to class.

Appendix B

Vasp2trace

In order to analyse the topology of a crystal, transformation properties of the Wannier functions[1] must be calculated, this procedure is explained in section 4.1. This requires a lot ot work if calculated by hand. However, fortunately the Bilbao Crystallographic Server [25, 26, 27] has useful tools to search topological insulators using VASP outputs. The program we used for this project is called 'Check Topological Mat' [5], and it has been developed based on the article [28].

This program takes as input a file denominated "trace.txt", which is calculated using the program "vasp2trace" (implemented in Fortran) and the output files obtained from a Band Structure calculation with VASP, the OUTCAR and WAVECAR files. However, the band structure is calculated in a particular k-path, determined by the maximal k-points[2] of the symmetry group. With this information the program "vasp2trace" creates the file "trace.txt" which has this structure:

1. The number of bands below the Fermi level. It should be clarified that if a gap exists in the band structure, the Fermi level does not exist, nevertheless, normally the chemical potential is referred to as the Fermi level in Solid State Physics, so whenever the Fermi level is mentioned this must be considerate.
2. A tag of 1 or 0 indicating if SOC is considered or not, respectively.
3. The number of symmetry operation of the group.
4. A table, with each line representing a symmetry operation. A general symmetry operation being $\{R \bigotimes S|\mathbf{t}\}$[3], it is represented as: R11,R12,...,R33,t1,t2,t3,Re(S11),Im(S11),...,Re(S22),Im(S22).
5. Number of maximal k-points and their coordinates.
6. For each maximal k-point, this information is presented in order. Number of symmetry operations of the little co-group of the k-point, then a list of indexes specifying which symmetry operation of the list above is part of the little co-group[4], and finally a table with each line specifying information for each band: number of bands below+1, degeneracy of the band, energy of the band in the k-point and the eigenvalues for each symmetry operation (real and imaginary part) of the little co-group.

As mentioned before, this file is delivered to the program [5] and it analyses whether the material is topological,trivial, an enforced semimetal... Thus this program will be really helpful in order to detect materials which are not trivial, since we will apply different pressure to our materials of interest, arising different properties.

[1] The Wannier functions are a set of orthogonal functions, which can be chosen to be localized. A further definition is provided in Appendix 4.1.

[2] A point $\mathbf{q}$ is maximal, if the site-symmetry group of that point ($G_{\mathbf{q}}$) is maximal. The site-symmetry group of a point $\mathbf{q}$ is a subgroup of the symmetry group G that leaves $\mathbf{q}$ invariant, and it is maximal if there is no other subgroup of G containing $G_{\mathbf{q}}$.

[3] In the general symmetry operation $\{R \bigotimes S|\mathbf{t}\}$, R is a orthonormal (3×3) matrix which is the symmetry operation acting on the real space, $\mathbf{t}$ is a 3D translation vector and S is the spin operation which is a (2×2) matrix.

[4] The little co-group of the point $\mathbf{q}$ is the group which leaves $\mathbf{q}$ invariant. $G_{\mathbf{q}} = \{G_{\mathbf{q}}\mathbf{q} = \mathbf{q} \mid G_{\mathbf{q}} \subset G\}$. This group combined with the translational group is called the little group.

Appendix C

Effective model

In section 7.3 the effective Hamiltonian $H(\mathbf{k})$ was given, which was constructed around the Γ point and determined to respect the symmetries, and defined with three matrices. In this manner, we give the exact form for each block, as well as the values for the fitting parameters, which were computed for the optical properties analysis in [21].

The matrix component related to the valence bands, which has two parameters α and v_F[1], has the form:

$$H_{2band} = \alpha|\mathbf{k}|^2\sigma_0 + v_F\mathbf{k}\cdot\sigma = \begin{pmatrix} \alpha|\mathbf{k}|^2 + v_F k_z & v_F(k_x - ik_y) \\ v_F(k_x + ik_y) & \alpha|\mathbf{k}|^2 - v_F k_z \end{pmatrix}, \tag{C.1}$$

Where σ_0 denotes the identity (2×2) and σ is a vector consisting of Pauli matrices. Similarly, the block describing conduction bands:

$$H_{4band} = v_F^1\mathbf{k}\cdot\lambda_1 + v_F^2\mathbf{k}\cdot\lambda_2 \tag{C.2}$$

$$= \begin{pmatrix} k_z v_F^1 & (k_x - ik_y)v_F^1 & \left(e^{-\frac{11i\pi}{12}}k_x + e^{-\frac{i\pi}{12}}k_y\right)v_F^2 & e^{-\frac{3i\pi}{4}}k_z v_F^2 \\ (k_x + ik_y)v_F^1 & -k_z v_F^1 & e^{\frac{3i\pi}{4}}k_z v_F^2 & \left(e^{\frac{7i\pi}{12}}k_x + e^{\frac{5i\pi}{12}}k_y\right)v_F^2 \\ \left(e^{\frac{11i\pi}{12}}k_x + e^{\frac{i\pi}{12}}k_y\right)v_F^2 & e^{-\frac{3i\pi}{4}}k_z v_F^2 & -k_z v_F^1 & (k_y - ik_x)v_F^1 \\ e^{\frac{3i\pi}{4}}k_z v_F^2 & \left(e^{-\frac{7i\pi}{12}}k_x + e^{-\frac{5i\pi}{12}}k_y\right)v_F^2 & (ik_x + k_y)v_F^1 & k_z v_F^1 \end{pmatrix}.$$

Where v_F^1 and v_F^2 are fitting parameters as well, and λ_i are complex Hermitian matrices that form a basis under which the Hamiltonian can be expanded. Finally, we define H_{cp} to describe transitions across the gap that connect the fourfold and twofold bands, parametrised by δ:

$$H_{cp} = \delta\begin{pmatrix} -k_x & e^{\frac{i\pi}{3}}k_y + e^{-\frac{5i\pi}{6}}k_z & -e^{\frac{5i\pi}{12}}k_y - e^{\frac{7i\pi}{12}}k_z & e^{\frac{i\pi}{4}}k_x \\ e^{\frac{i\pi}{3}}k_y - e^{-\frac{5i\pi}{6}}k_z & k_x & -ie^{\frac{i\pi}{4}}k_x & ie^{\frac{5i\pi}{12}}k_y - ie^{\frac{7i\pi}{12}}k_z \end{pmatrix}. \tag{C.3}$$

[1] v_F is known as the Fermi velocity, it is directly related to the viability of a DM detector as explained in [22].

	-1%	-2%	-3%
v_F^1	0.164	0.141	0.105
v_F^2	0.228	0.211	0.178
v_F	0.390	0.398	0.371
α	55.637	50.891	44.694
δ	0.370	0.587	0.690
Δ	0.009	0.030	0.056

Table C.1: Fitted values for different choices of lattice parameter compression. The units are expressed in terms of $\hbar = c = 1$ with $\vec{k}$ in units of $2\pi/a$, where $a = pa_0$, a_0 is the unperturbed lattice constant and $p = 0.99, 0.98, 0.97$ for 1%, 2%, 3% hydrostatic pressure respectively. It is important to remark that in units of c the Fermi velocities are of order $v_F \sim 10^{-4}c$.

Bibliography

[1] Jennifer Cano, Barry Bradlyn, Zhijun Wang, L. Elcoro, M. G. Vergniory, C. Felser, M. I. Aroyo, and B. Andrei Bernevig. Building blocks of topological quantum chemistry: Elementary band representations. 2017.

[2] D. Vanderbilt. *Berry Phases in Electronic Structure Theory: Electric Polarization, Orbital Magnetization and Topological Insulators*. Cambridge University Press, 2018.

[3] János K Asbóth, László Oroszlány, and András Pályi. A short course on topological insulators. *Lecture notes in physics*, 919, 2016.

[4] J. Zak. Symmetry specification of bands in solids. *Phys. Rev. Lett.*, 45:1025–1028, Sep 1980.

[5] Dgenpos. `http://www.cryst.ehu.es/cgi-bin/cryst/programs/topological.pl`.

[6] Felix Flicker, Fernando de Juan, Barry Bradlyn, Takahiro Morimoto, Maia G. Vergniory, and Adolfo G. Grushin. Chiral optical response of multifold fermions. 2018.

[7] Jean-Pierre Serre. *Linear representations of finite groups*. Springer-Verlag, New York, 1977. Translated from the second French edition by Leonard L. Scott, Graduate Texts in Mathematics, Vol. 42.

[8] Georg Kresse and Jürgen Hafner. Ab initio molecular dynamics for liquid metals. *Physical Review B*, 47(1):558, 1993.

[9] G. Kresse and J. Hafner. Ab initio molecular-dynamics simulation of the liquid-metal–amorphous-semiconductor transition in germanium. *Phys. Rev. B*, 49:14251–14269, May 1994.

[10] G. Kresse and J. FurthmÃ$\frac{1}{4}$ller. Efficiency of ab-initio total energy calculations for metals and semiconductors using a plane-wave basis set. *Computational Materials Science*, 6(1):15 – 50, 1996.

[11] G. Kresse and J. Furthmüller. Efficient iterative schemes for ab initio total-energy calculations using a plane-wave basis set. *Phys. Rev. B*, 54:11169–11186, Oct 1996.

[12] Richard M Martin. *Electronic structure: basic theory and practical methods*. Cambridge university press, 2004.

[13] Peter Schwerdtfeger. The pseudopotential approximation in electronic structure theory. *ChemPhysChem*, 12(17):3143–3155, 2011.

[14] Ersen Mete. Electronic properties of transition metal oxides. `https://www.researchgate.net/publication/33575690_Electronic_Properties_of_Transition_Metal_Oxides`, 06 2019.

[15] John P. Perdew and Yue Wang. Accurate and simple analytic representation of the electron-gas correlation energy. *Phys. Rev. B*, 45:13244–13249, Jun 1992.

[16] John P. Perdew, Kieron Burke, and Matthias Ernzerhof. Generalized gradient approximation made simple. *Phys. Rev. Lett.*, 77:3865–3868, Oct 1996.

[17] N.W. Ashcroft and N.D. Mermin. *Solid State Physics*. Cengage Learning, 2011.

[18] Koichi Momma and Fujio Izumi. Vesta: A three-dimensional visualization system for electronic and structural analysis. *Journal of Applied Crystallography - J APPL CRYST*, 41:653–658, 06 2008.

[19] Anubhav Jain, Shyue Ping Ong, Geoffroy Hautier, Wei Chen, William Davidson Richards, Stephen Dacek, Shreyas Cholia, Dan Gunter, David Skinner, Gerbrand Ceder, and Kristin a. Persson. The Materials Project: A materials genome approach to accelerating materials innovation. *APL Materials*, 1(1):011002, 2013.

[20] YX Zhao and Andreas P Schnyder. Nonsymmorphic symmetry-required band crossings in topological semimetals. *Physical Review B*, 94(19):195109, 2016.

[21] Miguel-Ángel Sánchez-Martínez, Iñigo Robredo, Arkaitz Bidaurrazaga, Aitor Bergara, Fernando de Juan, Adolfo G. Grushin, and Maia G. Vergniory. Spectral and optical properties of $Ag_3Au(Se_2,Te_2)$ and dark matter detection, 2019.

[22] Yonit Hochberg, Yonatan Kahn, Mariangela Lisanti, Kathryn M Zurek, Adolfo G Grushin, Roni Ilan, Sinead M Griffin, Zhen-Fei Liu, Sophie F Weber, and Jeffrey B Neaton. Detection of sub-mev dark matter with three-dimensional dirac materials. *Physical Review D*, 97(1):015004, 2018.

[23] Frank Herman, Charles D. Kuglin, Kermit F. Cuff, and Richard L. Kortum. Relativistic corrections to the band structure of tetrahedrally bonded semiconductors. *Phys. Rev. Lett.*, 11:541–545, Dec 1963.

[24] Emilia Morosan, Henny Zandbergen, Lu Li, Minhyea Lee, J G. Checkelsky, M Heinrich, T Siegrist, N P. Ong, and R J. Cava. Sharp switching of the magnetization in $Fe_{1/4}$ TaS_2. *Phys. Rev. B*, 75, 03 2007.

[25] D. Orobengoa E. Tasci G. de la Flor A. Kirov M. I. Aroyo, J. M. Perez-Mato. Crystallography online: Bilbao crystallographic server. *Bulg. Chem. Commun.*, 43(2):183–197, 2011.

[26] C. Capillas E. Kroumova S. Ivantchev G. Madariaga A. Kirov H. Wondratschek M. I. Aroyo, J. M. Perez-Mato. Bilbao crystallographic server i: Databases and crystallographic computing programs. *Z. Krist.*, 221(1):15–27, 2006.

[27] C. Capillas J. M. Perez-Mato H. Wondratschek M. I. Aroyo, A. Kirov. Bilbao crystallographic server ii: Representations of crystallographic point groups and space groups. *Acta Cryst.*, A26:115–128, 2006.

[28] M. G. Vergniory, L. Elcoro, Claudia Felser, Nicolas Regnault, B. Andrei Bernevig, and Zhijun Wang. A complete catalogue of high-quality topological materials. *Nature*, 566(7745):480–485, 2019.